

# Promoting extinction or minimizing growth? The impact of treatment on trait trajectories in evolving populations

Michael Raatz\*<sup>1</sup> and Arne Traulsen<sup>1</sup>

<sup>1</sup>Department for Evolutionary Theory, Max Planck Institute for Evolutionary Biology, Plön, Germany

When cancers or bacterial infections establish, small populations of cells have to free themselves from homeostatic regulations that prevent their expansion. Trait evolution allows these populations to evade this regulation, escape stochastic extinction and climb up the fitness landscape. In this study, we analyse this complex process and investigate the fate of a cell population that underlies the basic processes of birth, death and mutation. We find that the shape of the fitness landscape dictates a circular adaptation trajectory in the trait space spanned by birth and death rates. We show that successful adaptation is less likely for parental populations with higher turnover (higher birth and death rates). Including density- or trait-affecting treatment we find that these treatment types change the adaptation dynamics in agreement with a geometrical analysis of fitness gradients. Treatment strategies that simultaneously target birth and death rates are most effective, but also increase evolvability. By mapping physiological adaptation pathways and molecular drug mechanisms to traits and treatments with clear eco-evolutionary consequences, we can achieve a much better understanding of the adaptation dynamics and the eco-evolutionary mechanisms at play in the dynamics of cancer and bacterial infections.

Keywords: Evolutionary rescue, Resistance evolution, Dormancy, Competitive release, Immune evasion

## Contents

<b>1. Introduction</b>	<b>2</b>
<b>2. Methods</b>	<b>4</b>
2.1. Description of the underlying microscopic processes . . . . .	4
2.2. Stochastic model . . . . .	5
2.3. Deterministic model . . . . .	6
2.4. Defining fitness . . . . .	7
2.5. Treatment types . . . . .	9
<b>3. Results</b>	<b>12</b>
3.1. Trajectories of adaptation in untreated populations . . . . .	12
3.2. Trajectories of adaptation in treated populations . . . . .	15
3.3. Which fitness component is more important? . . . . .	21
<b>4. Discussion</b>	<b>24</b>
<b>A. Supplement</b>	<b>37</b>
A.1. Derivation of survival probability fitness component . . . . .	37
A.2. Supplementary Figures . . . . .	38

---

\*mraatz@evolbio.mpg.de

# 38 1. Introduction

39 Cancer cells and bacterial pathogens show extensive adaptive potential, which helps them to establish  
40 even in unfavourable conditions and outgrow competitors and external pressures, for example by the  
41 immune system (Fridman et al., 2012; Winstanley et al., 2016). In healthy tissue or healthy micro-  
42 biomes, external regulation aims to maintain a constant population size, which together with stochastic  
43 fluctuations in the population dynamics of individual subpopulations results in a constant turnover  
44 characterized by the eventual stochastic extinction of a specific subpopulation and subsequent replace-  
45 ment by other subpopulations (Gallaher et al., 2019). This extinction can be prevented by adaptations  
46 that give an emerging subpopulation of cells a fitness advantage over the remaining population. The  
47 increased fitness reduces the subpopulation's risk of extinction in a process often termed evolutionary  
48 rescue (Orr and Unckless, 2008; Alexander et al., 2014; Uecker et al., 2014; Marrec and Bitbol, 2020a).  
49 Accordingly, the onset of cancer is characterized by malignant cells breaking with the homeostatic  
50 regulation of healthy tissue (Basanta and Anderson, 2013, 2017). Similarly, bacterial infections that  
51 either emerge from or invade an otherwise healthy microbiome have to develop mechanisms to out-  
52 grow the other community members and free themselves from regulative community interactions, for  
53 example by pathoadaptive mutations (Winstanley et al., 2016; Culyba and Tyne, 2021).

54 Many individual mechanisms of how this fitness increase is realized have been identified. In a pro-  
55 gressing tumour, the net growth increase of subclones relative to their parental clones often indicates a  
56 continuing evolution towards higher net growth rates, often but not always driven by the accumulation  
57 of known driver mutations (Gruber et al., 2019). Biswas et al. (2004) suggest that NF- $\kappa$ B activation  
58 increases proliferation and decreases apoptosis rate in estrogen receptor-negative breast cancer cells.  
59 Lopez and Tait (2015) describe how apoptosis is avoided in cancer cells by upregulating anti-apoptotic  
60 BCL-2 proteins. Similarly, also infectious bacteria must adapt during an ongoing infection (Faure et al.,  
61 2018; Culyba and Tyne, 2021). For example, Young et al. (2017) showed that formerly commensal  
62 constituents of the host microbiome accrue substantial adaptive genotypic changes as they become

63 infective, and [Both et al. \(2021\)](#) documented the phenotypic changes during the adaptation to the  
64 host environment.

65 These adaptations have ~~lead~~led to the development of drugs that target many such mechanisms  
66 both in cancer and in bacterial infections. For example, BCL-2 inhibitors aim to counter decreased  
67 apoptosis rates in cancer cells ([Montero and Letai, 2018](#)), and NF- $\kappa$ B inhibition is investigated to lessen  
68 the inflammatory increase in proliferation ([Yu et al., 2020](#)). Anti-virulence therapy and microbiome  
69 modulation have been proposed as options besides antibiotics to counter the adaptations of pathogenic  
70 bacteria ([Hauser et al., 2016](#)).

71 The diversity of these specific, experimentally well-characterized adaptations and potential treatments  
72 call for an abstraction to elucidate the eco-evolutionary mechanisms behind adaptations of cell pop-  
73 ulations in challenging environments. It is a priori unclear which functional traits of cancer cells or  
74 pathogenic bacteria would be targeted by adaptations. Similarly, it is not understood how treatment-  
75 induced perturbations to the adapting populations or their environments would affect the adaptation  
76 process. In order to generalize from the plethora of adaptive mutations or plastic responses of cancer  
77 cells and bacterial pathogens, we describe the population of evolving cells in a minimal model: Cells  
78 competitively grow, die and mutate. We speculate that many of the adaptive mechanisms described  
79 above can be classified as either increasing the birth rate or decreasing the death rate. Treatment  
80 approaches that try to contain or eradicate such adapting populations could then be grouped into two  
81 types: (i) They either directly decrease the population size of the target population, or (ii) indirectly  
82 decrease the population size by affecting their birth and death rates. In such a simplistic but general  
83 setting we investigate where adaptation will take the population in a trait space spanned by birth rate  
84 and death rate, and how treatment will affect the resulting adaptation trajectories.

## 85 2. Methods

### 86 2.1. Description of the underlying microscopic processes

87 We represent the initial phases of tumour formation or the establishment of a bacterial infection as  
88 the spread of a population of cells in a harsh environment. In our model, this harshness manifests in  
89 similar birth and death rates and a decreasing birth rate as population size increases. The similarity  
90 of birth and death rates is supported by the high proportion of dead cells in tumours (Kerr and  
91 Lamb, 1984; de Jong et al., 2000; Liu et al., 2001; Alenzi, 2004; Gallaher et al., 2019). While bacterial  
92 death rates in benign conditions are small (Koch, 1959; Stewart et al., 2005) the mortality from  
93 immune responses or nutrient scarcity may be considerable and the importance of bacterial death is  
94 probably underestimated (Frenoy and Bonhoeffer, 2018). ~~Space~~Oxygen availability, space restriction  
95 and nutrient limitation are likely mechanisms for the density dependence of the birth rate. We assume  
96 that this density dependence restricts the birth rate  $\beta$  of cells by a logistic term with a carrying  
97 capacity  $K$ . We assume that death occurs at a constant rate  $\delta$ . Upon each birth event mutations can  
98 give rise to lineages with trait combinations  $(\beta_m, \delta_m)$  that slightly deviate from those of their parental  
99 lineage. We assume that mutations in the two traits can occur independently and without correlation,  
100 and that mutational effects are purely additive. The birth and expansion of fitter mutants can shift  
101 the population average trait combination and thus cause the population to adapt by exploring its  
102 adaptive landscape (e.g. Patout et al., 2021). We can represent the adaptation of a population by the  
103 trajectory of the mean trait combination in the trait space spanned by birth rate  $\beta$  and death rate  
104  $\delta$ . Focussing on the initial phases of adaptation, we assume that the carrying capacity  $K$  remains  
105 constant. We will investigate treatment types that either target the density or the traits of the  
106 evolving population (Fig. 1). Density-affecting treatment types are modelled as instantaneous density  
107 reductions (bottlenecks) applied homogeneously to the whole population, similar to the resection of  
108 a tumour where cancerous tissue is surgically removed, or the voiding of the bladder during urinary  
109 tract infections where most non-attached pathogenic bacteria are flushed out (Cox and Hinman, 1961;

**Table 1 Reference parameter set.** The parameters of the stochastic adaptive process are chosen such that without treatment about half of the replicate simulations show successful adaptation. The parameters of the deterministic model were set such that the time scales of the deterministic dynamics would match the time scales of the stochastic model. Deviations from these values are reported where applicable.

Parameter	Biological meaning	Value
$\beta_0$	Birth rate of the first parental lineage	1
$\delta_0$	Death rate of the first parental lineage	1
$K$	Carrying capacity for total cell population	20 000
$\Delta$	Absolute treatment effect in trait space	0.5
$N_0$	Initial size of the first parental lineage	100
$dt$	Time step for evaluation of stochastic dynamics	0.1
$\mu$	Mutation probability per cell division	0.005
$\sigma$	Standard deviation of mutational trait changes	0.05
$G_\beta$	Genetic variance of <del>death</del> -birth rate	$10^{-2.5}$
$G_\delta$	Genetic variance of death rate	$10^{-2.5}$
$c$	Trait change deceleration for small trait values	0.1

110 [Sobel, 1997](#)). Trait-affecting treatment types are implemented by prolonged additive changes to either  
 111 the birth or the death rates of the individual lineages. ‘Static’ drugs decrease the birth rate by  $\Delta_\beta$   
 112 (e.g. cytostatic chemotherapy or bacteriostatic antibiotics), ‘toxic’ drugs increase the death rate by  
 113  $\Delta_\delta$  (e.g. cytotoxic chemotherapy, immunotherapy or bactericidal antibiotics). Different trait-affecting  
 114 treatment types can thus be represented by vectors  $(\Delta_\beta, \Delta_\delta)$  in trait space (Fig. 1). Accounting for  
 115 treatment and logistic density dependence of birth rates the effective birth and death rates of lineage  
 116  $i$  with population size  $N_i$  are given by

$$\begin{aligned}
 b_i(t) &= (\beta_i - \Delta_\beta(t)) \left( 1 - \frac{\sum_j N_j(t)}{K} \right) \\
 d_i(t) &= \delta_i + \Delta_\delta(t)
 \end{aligned}
 \tag{1}$$

117 We ensure that effective birth rates are always greater than or equal to zero, setting them to zero if  
 118 they would be negative.

## 119 2.2. Stochastic model

120 We use these microprocesses of birth, death and mutation to construct a discrete-time stochastic model  
 121 (Eq. 2). We assume that the number of birth and death events per lineage  $i$  per time step  $dt$ ,  $(B_i(t+dt)$

122 and  $D_i(t + dt)$  are Poisson-distributed around the expected numbers of birth events  $b_i N_i dt$  and death  
 123 events  $d_i N_i dt$ , given the effective birth and death rates  $b_i$  and  $d_i$  according to Eq. (1). The number  
 124 of mutants  $M_i(t + dt)$  among the new-born cells is given by a binomial distribution with mutation  
 125 probability  $\mu$ .

$$\begin{aligned}
 B_i(t + dt) &\sim \text{Poisson}(b_i(t) N_i(t) dt) \\
 D_i(t + dt) &\sim \text{Poisson}(d_i(t) N_i(t) dt) \\
 M_i(t + dt) &\sim \text{Binomial}(B_i(t + dt), \mu) \\
 N_i(t + dt) &= N_i(t) + B_i(t + dt) - D_i(t + dt) - M_i(t + dt)
 \end{aligned}
 \tag{2}$$

126 Each newly mutated cell founds a new lineage with trait values drawn from a truncated Gaussian  
 127 distribution with the parental trait values as the mean and a standard deviation of  $\sigma = 0.05$ . By  
 128 setting the lower bound of the truncated Gaussian distribution to zero, we prevent the evolution of  
 129 negative trait values. The upper bound was set to 1000, which is far beyond the trait values that are  
 130 obtained in our simulations and thus does not affect our results. By ~~drawing assuming a truncated~~  
 131 Gaussian distribution of mutational effects we draw the mutant trait values predominantly from the  
 132 vicinity of the parental traits. Thus, we focus our investigation on an adaptive process where trait  
 133 changes occur predominantly in small steps, either by plastic changes to the cell phenotypes or by  
 134 mutations with small effects, albeit single large-effect jackpot events are also possible but much less  
 135 likely. This represents the diversity of adaptive mechanisms in cancer and pathoadaptations in bacterial  
 136 infections resulting from the multitude of stressors that adapting cell populations face in the human  
 137 body.

### 138 2.3. Deterministic model

139 Defining the total population size as  $N(t) = \sum_i N_i(t)$  and the population average traits as  $\bar{\beta}(t) =$   
 140  $\sum_i \beta_i N_i(t)/N(t)$  and  $\bar{\delta}(t) = \sum_i \delta_i N_i(t)/N(t)$ , we can construct a deterministic model from the above  
 141 microscopic model using a Quantitative Genetics approach (Lande, 1982),

$$\begin{aligned}
\frac{dN(t)}{dt} &= \left( (\bar{\beta}(t) - \Delta_{\beta}(t)) \left( 1 - \frac{N(t)}{K} \right) - (\bar{\delta}(t) + \Delta_{\delta}(t)) \right) N(t) \\
\frac{d\bar{\beta}(t)}{dt} &= G_{\beta} \frac{\partial \varphi(t)}{\partial \bar{\beta}(t)} e^{-c/\bar{\beta}(t)} \\
\frac{d\bar{\delta}(t)}{dt} &= G_{\delta} \frac{\partial \varphi(t)}{\partial \bar{\delta}(t)} e^{-c/\bar{\delta}(t)}
\end{aligned} \tag{3}$$

142 Here, the change in total population size is governed by the difference of logistic average birth rate and  
143 average death rate. Treatment affects the effective birth and death rates as in Eq. (1). The change in  
144 the average birth and death rates are assumed to be proportional to the gradient of a function  $f(t)$   
145  $\varphi(t)$  (defined below) that describes the fitness of individuals with proportionality constants  $G_{\beta}$  and  $G_{\delta}$   
146 that describe the additive genetic variance in the traits (Lande, 1982). The factors  $e^{-c/\bar{\beta}(t)}$  and  $e^{-c/\bar{\delta}(t)}$   
147 ensure decelerating trait changes close to the trait axis, thus preventing negative trait values (Abrams  
148 and Matsuda, 1997; Raatz et al., 2019). Note that also this deterministic model formulation assumes  
149 independence of the two traits. The system of ordinary differential equations Eq. 3 is numerically  
150 integrated using the LSODA implementation of the solve\_ivp function from the Scipy library (Virtanen  
151 et al., 2020) in Python (version 3.8). Standard initial conditions are  $N(0) = 100$ ,  $\bar{\beta}(0) = 1$ ,  $\bar{\delta}(0) = 1$  -  
152 (Tab. 1).

153 Setting the temporal derivative of the population size to zero we can obtain the conditions for the  
154 manifold where the population change equals zero. On this manifold, the population size is given by  
155 the effective carrying capacity

$$N^*(t) = K \left( 1 - \frac{\bar{\delta}(t) + \Delta_{\delta}(t)}{\bar{\beta}(t) - \Delta_{\beta}(t)} \right). \tag{4}$$

156 Because of treatment, the effective carrying capacity could become negative. In our simulations,  
157 however, we ensure that the population size remains bounded by zero.

## 158 2.4. Defining fitness

159 Adaptation should increase fitness relative to competitors, but what exactly determines fitness in  
160 populations that have to adapt to unfavourable conditions? Generally, defining fitness measures is

161 ~~not unambiguous~~ ambiguous (Doebeli et al., 2017; Kokko, 2021). One possible definition is lifetime-  
 162 reproductive output, which itself is a composite measure that includes net growth rate, but also the  
 163 probability that newly founded lineages survive stochastic population size fluctuations. Even in our  
 164 simplified setting the determinants of fitness are a priori not trivial, particularly in a regime of high  
 165 rates of stochastic extinction of lineages. An obvious choice may be the net growth of a lineage  $r$ ,  
 166 which determines how quickly that lineage grows out of this regime of probable stochastic extinction  
 167 and outcompetes other lineages. Similarly, the survival probability of a newly founded lineage  $p$  may  
 168 be selected for. Also, the importance of these two fitness components may change with population  
 169 size, with survival probability being more important at small lineage size and net growth becoming  
 170 more decisive for larger lineage sizes. We define these two measures of fitness as

$$r_i(t) = (\beta_i - \Delta_\beta(t)) \left(1 - \frac{N(t)}{K}\right) - (\delta_i + \Delta_\delta(t)) \quad \text{Lineage net growth} \quad (5)$$

$$p_i(t) = \begin{cases} 1 - \frac{\delta_i + \Delta_\delta(t)}{(\beta_i - \Delta_\beta(t)) \left(1 - \frac{N(t)}{K}\right)} & \text{if } \frac{\delta_i + \Delta_\delta(t)}{(\beta_i - \Delta_\beta(t)) \left(1 - \frac{N(t)}{K}\right)} \leq 1 \\ 0 & \text{if } \frac{\delta_i + \Delta_\delta(t)}{(\beta_i - \Delta_\beta(t)) \left(1 - \frac{N(t)}{K}\right)} \geq 1 \end{cases} \quad \text{Survival probability of newly founded lineage} \quad (6)$$

171 The survival probability here follows from a simplified branching process under the assumption that  
 172 during the potential establishment of a mutant lineage, the population size of the remaining population  
 173 will stay approximately constant (see Supplementary Section A.1). Assuming a large carrying capacity  
 174  $K$ , the density dependence vanishes and the survival probability becomes equal to one minus the  
 175 extinction probability for newly founded lineages as derived by others (Xue and Leibler, 2017; Coates  
 176 et al., 2018; Marrec and Bitbol, 2020b).

177 We numerically confirmed the agreement of the survival probability definition with simulations of our  
 178 model for the case of no mutation ( $\mu = 0$ ) (Fig. S1). Note that the fraction of birth rate over death rate  
 179 has also been proposed as a fitness measure for a model that is identical to ours, but lacks mutations  
 180 (Parsons and Quince, 2007).

181 Adaptation will either be driven by selection for the fittest lineage in the stochastic model or determined  
 182 by the fitness gradient in the deterministic model. In both cases, adaptation manifests as a changing



183 average population trait combination. The direction of adaptation in trait space should be determined  
 184 by the gradients of the two fitness components in the absence of treatment. We can compute those  
 185 gradients as

$$\nabla r_i = \begin{pmatrix} \frac{\partial r_i}{\partial \beta_i} \\ \frac{\partial r_i}{\partial \delta_i} \end{pmatrix} = \begin{pmatrix} 1 - \frac{\sum_i N_i}{K} \\ -1 \end{pmatrix} \quad (7)$$

$$\nabla p_i = \begin{pmatrix} \frac{\partial p_i}{\partial \beta_i} \\ \frac{\partial p_i}{\partial \delta_i} \end{pmatrix} = \frac{1}{\beta_i \left(1 - \frac{\sum_i N_i}{K}\right)} \begin{pmatrix} \frac{\delta_i}{\beta_i} \\ -1 \end{pmatrix} \quad (8)$$

186 In the deterministic model (Eq. 3) we explicitly prescribe whether adaptation should follow the net  
 187 growth or the survival probability fitness gradient and thus substitute  $f(t) - \varphi(t)$  by  $r(t)$  or by  $p(t)$ . If  
 188 adaptation is determined by net growth we obtain

$$\begin{pmatrix} \frac{\partial \varphi(t)}{\partial \beta(t)} \\ \frac{\partial \varphi(t)}{\partial \delta(t)} \end{pmatrix} = \begin{pmatrix} \frac{\partial r(t)}{\partial \beta(t)} \\ \frac{\partial r(t)}{\partial \delta(t)} \end{pmatrix} = \begin{pmatrix} 1 - \frac{N}{K} \\ -1 \end{pmatrix}$$

189 If adaptation is driven by survival probability we obtain

$$\begin{pmatrix} \frac{\partial \varphi(t)}{\partial \beta(t)} \\ \frac{\partial \varphi(t)}{\partial \delta(t)} \end{pmatrix} = \begin{pmatrix} \frac{\partial p(t)}{\partial \beta(t)} \\ \frac{\partial p(t)}{\partial \delta(t)} \end{pmatrix} = \frac{1}{\beta(t) \left(1 - \frac{N}{K}\right)} \begin{pmatrix} \frac{\delta(t)}{\beta(t)} \\ -1 \end{pmatrix}$$

## 190 2.5. Treatment types

191 Treatment can either immediately kill part of the population or rig the chances of a population to  
 192 grow by decreasing birth rates or increasing death rates (Fig. 1). The first case, which affects density  
 193 directly, causes a direct, instantaneous population size reduction. The second case, which affects traits,  
 194 brings about an indirect, gradual population size decline where on average more death events than  
 195 birth events occur. These two treatment types thus differ in their temporal structure. Whereas the first  
 196 treatment occurs instantaneously, the latter treatment is applied for a defined time span, during which  
 197 the treatment alters the effective birth and death rates of cells, similar to (Marrec and Bitbol, 2020b).  
 198 We assume that the density-affecting treatment type targets all cells homogeneously, irrespective of  
 199 their traits. The additive trait changes during trait-affecting treatment are also equally applied to all  
 200 lineages, resulting in different relative trait changes, depending on the trait values of each lineage. We

201 represent different trait-affecting treatment types as vectors of length  $\Delta$  in trait space with components  
 202 given in Fig. 1. Besides the pure, static (affecting birth rates only, horizontal) or toxic (affecting death  
 203 rates only, vertical) treatments, we account for the fact that the boundaries between static or toxic  
 204 treatment are often blurred. The same drug can be static or toxic, depending on the dose (Masuda  
 205 et al., 1977), or treatment intentionally consists of two different drug types that each act more static or  
 206 toxic (Coates et al., 2018; Jaaks et al., 2022). Thus, we include a mixed treatment where both treatment  
 207 vector components  $\Delta_\beta$  and  $\Delta_\delta$  have the same length. Additionally, we propose two treatment types  
 208 that also combine static and toxic components ~~and~~ but additionally account for the shape of the  
 209 fitness landscape ~~by countering either~~. The minimizing growth treatment counters the net growth  
 210 rate fitness gradient (~~minimizing growth~~) ~~or the~~ Eq. 7) and has vector components  $(\Delta_\beta, \Delta_\delta) \propto \nabla \overline{r(t)}$   
 211 where  $\overline{r(t)}$  is the average net growth rate of the population at time  $t$ . The maximizing extinction  
 212 treatment counters the survival probability fitness gradient (~~maximizing extinction~~) Eq. 8) and has  
 213 vector components  $(\Delta_\beta, \Delta_\delta) \propto \nabla \overline{p(t)}$  where  $\overline{p(t)}$  is the average survival probability of the population  
 214 at time  $t$ . The minimizing growth treatment components are density-dependent, the maximizing  
 215 extinction treatment components are trait-dependent, i.e. a function of the population average trait  
 216 combination (Fig. 1).

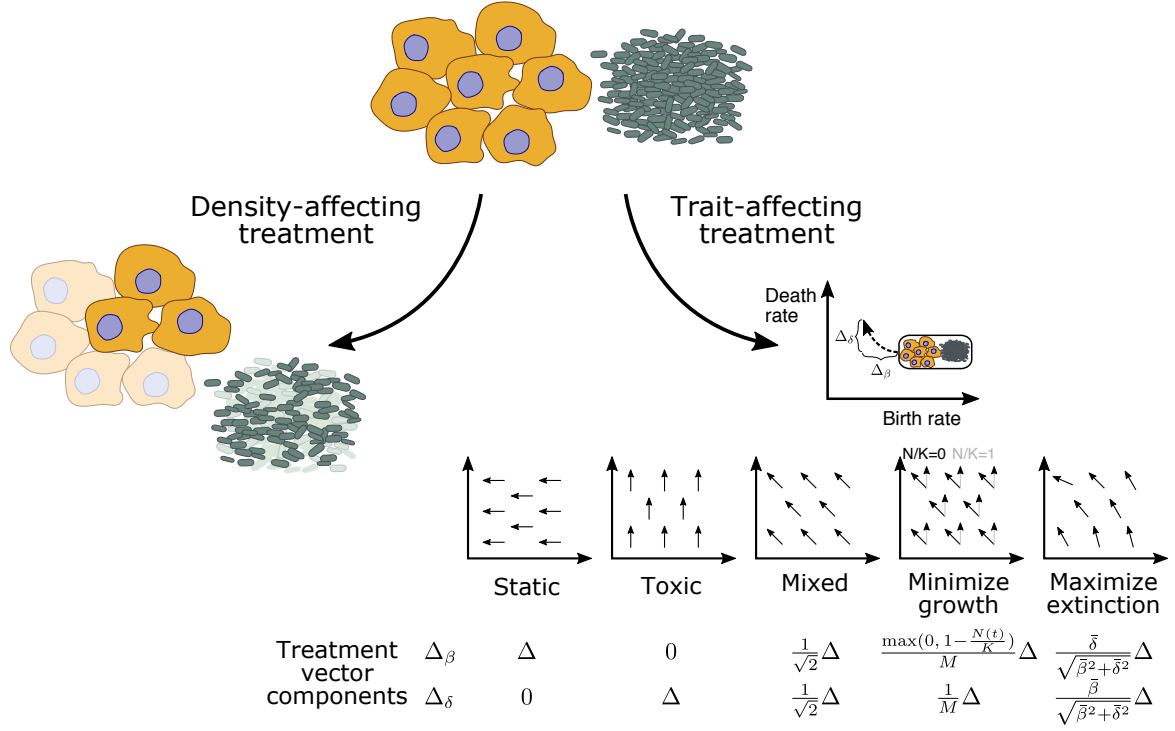


**Figure 1** Different treatment types can either affect the cell density directly (left) or indirectly via changing the traits (right). Populations of cancer cells (yellow) or pathogenic bacteria (green) can be targeted with different mechanisms. Density-affecting treatment applies a bottleneck and reduces the population size instantaneously to a fraction  $f$ . Trait-affecting treatment, e.g. chemotherapy, alters the traits for a prolonged time period (the treatment duration) and displaces the population in trait space temporarily which results in population decline. Note that  $M = \sqrt{1 + \max(0, 1 - N(t)/K)^2}$  is a normalization factor.

## 217 3. Results

### 218 3.1. Trajectories of adaptation in untreated populations

219 When suddenly faced with challenging environments, rapidly proliferating cell populations can quickly  
220 adapt by acquiring mutations ~~or leveraging phenotypic plasticity~~, often resulting in continuing popula-  
221 tion growth. We represent the resulting phenotypic changes as changed trait values of offspring lineages  
222 relative to the trait values of their parental lineages. Such phenotypic adaptations allow for population  
223 size increases and realize a continuously changing average population trait combination (Fig. 2). The  
224 population size increases are characterized by a succession of fitter and fitter lineages that raise the  
225 effective carrying capacity  $N^*$  (Eq. 4), which allows the population size to increase further. Thus trait  
226 adaptation acts as a rubber band here that is extended by adaptive steps and contracts as growth  
227 closes the gap between population size and effective carrying capacity. The adaptive steps form a trait  
228 space trajectory that travels from the trait combination of the initial parental lineage to smaller death  
229 rates and larger birth rates.

230 We hypothesize that this trajectory is the outcome of the stochastic exploration of trait space that  
231 climbs up a fitness landscape, with fitter lineages out-competing less fit lineages. This fitness landscape  
232 can be characterized by fitness gradients and we propose net growth rate and survival probability as  
233 potential fitness components that generate these gradients. For our model, we see that the gradients  
234 of these two fitness components are not necessarily aligned. The vector representations of the net  
235 growth rate fitness gradient are parallel throughout trait space, indicating higher net growth rates for  
236 high birth rates and low death rates, resulting in a unidirectional, trait-independent fitness gradient  
237 (Fig. 3a). The vector representations of the survival probability fitness gradient form a circular vector  
238 field, indicating a trait-dependent fitness gradient with higher survival probability for high birth rates  
239 and low death rates (Fig. 3b).

240 The direction of the gradient of net growth  $\nabla r$  is density-dependent, i.e. it changes with population  
241 size (Eq. 7). The direction of the gradient of survival probability  $\nabla p$  does not depend on population

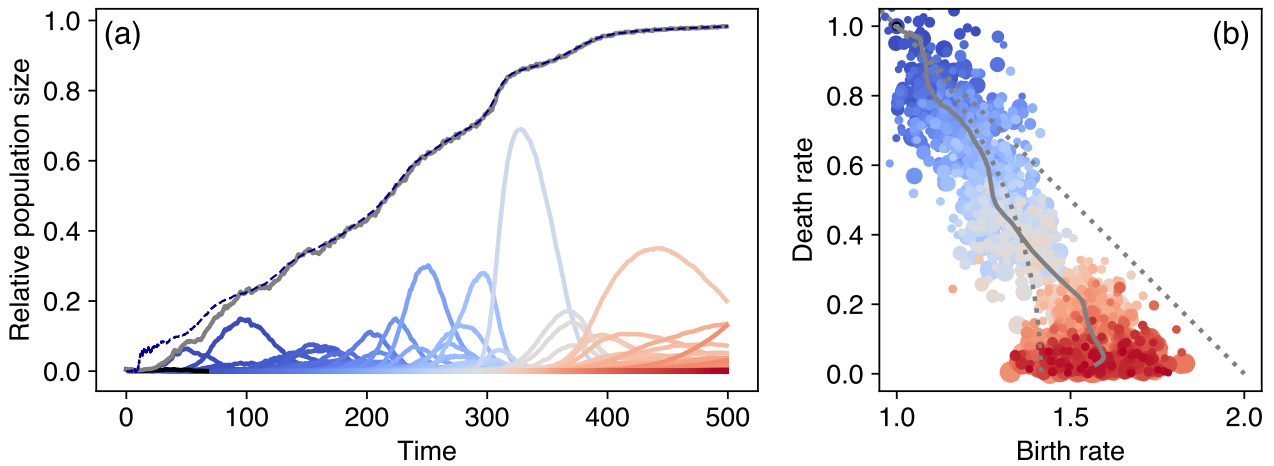


**Figure 2 Exemplary population and trait dynamics for adaptation in challenging environments.** (a) Starting from small initial numbers ( $N_0/K = 0.01$ ) the total population size (grey line) relative to the carrying capacity,  $N(t)/K$ , increases in a succession of fitter and fitter lineages (depicted by the blue-to-red colors indicating the order of appearance). For clarity, we show here only those lineages that persist for more than 10 time units. The dashed line shows the effective carrying capacity where population change is zero in the deterministic model (Eq. 4). The appearance of fitter lineages increases the effective carrying capacity and allows for a further increase in population size. (b) The trait combination of each lineage in panel (a) is shown here with the same color coding, with the grey line now depicting the population average. The point size is determined by the persistence time of a lineage relative to the longest persistence time. Starting from challenging conditions of birth rate  $\beta_0 = 1$  and death rate  $\delta_0 = 1$  the population average trait combination (grey line) travels through trait space describing the trait space trajectory of adaptation. The dotted grey lines represent the net growth fitness gradient at small population sizes (straight line) and the survival probability fitness gradient (circular line).

242 size but is trait-dependent (Eq. 8). Interestingly, we find that both fitness gradients are parallel  
 243 as soon as the manifold of zero population size change is reached and the population size equals  
 244 the effective carrying capacity,  $N(t) = N^*$  (Eq. 4, Fig. 3). Therefore, only in the initial phases of  
 245 adaptation (Fig. 2a), or during and short after treatment when the population size deviates from  $N^*$   
 246 the two fitness components may have non-parallel directions and thus differently affect the direction  
 247 of adaptation steps. As soon as the total population size reaches  $N^*$ , the effects of the two fitness  
 248 components cannot be disentangled, leaving us to conclude that they together dictate the trajectory  
 249 of trait adaptation.

250 Successful adaptation in unfavourable conditions is a stochastic event. When starting with an initial  
 251 wildtype population size of  $N_0 > 0$  and equal birth and death rate, the net growth rate is negative

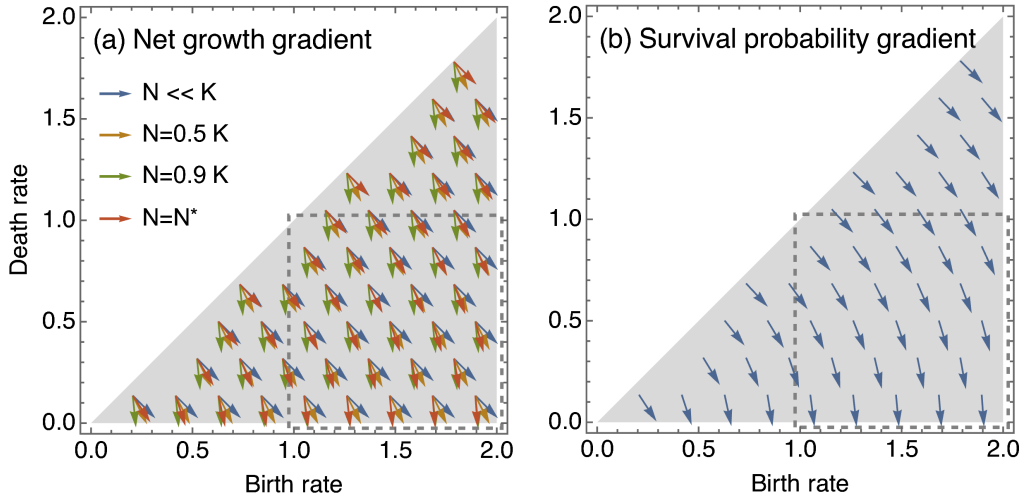


**Figure 3 Predicted adaptation directions in trait space.** (a) The direction of the net growth gradient is density-dependent, but trait-independent (Eq. (7)). (b) The direction of the survival probability gradient is density-independent, but trait-dependent and has a circular shape (Eq. (8)). At the effective carrying capacity  $N^*$ , depicted by the red arrows in panel (a), the net growth fitness gradient is parallel to the survival probability fitness gradient. Note that the effective carrying capacity depends on the traits, this causes the apparent trait dependence of the net growth gradient at effective carrying capacity. Given these gradients and initial parental lineages starting from  $\beta_0 = \delta_0 = 1$  the trait trajectories are moving mainly within the region of trait space enclosed by the grey dashed rectangle. Therefore, we zoom in on this region when visualizing trait space trajectories such as in Fig. 2.

252 and the survival probability is zero (Eqs. 5, 6). Thus, the wildtype lineage inevitably goes extinct in  
 253 our model, and population survival can only be achieved by adaptation and the succession of fitter  
 254 lineages as described above, i.e. evolutionary rescue. The success of this adaptive process and its  
 255 average trajectory can be depicted by combining a large number (1000) of independent replicates  
 256 (Figs. 4, 5). We find that moving the trait combination of the first parental lineage further to the  
 257 upper right corner of trait space, and thus increasing both the initial birth and death rate equally,  
 258 increases the number of extinct replicate populations, indicating a lower probability of successful  
 259 adaptation and evolutionary rescue. As expected, we find that a larger initial parental population  
 260 and a higher mutation probability per birth event ~~and a larger initial parental population~~ increase the  
 261 rescue probability as this increases both the ~~rate at pool from~~ rate at which they appear and the ~~pool~~  
 262 ~~from which they can emerge~~ can emerge and rate at which they appear (Figs. 4, S2).

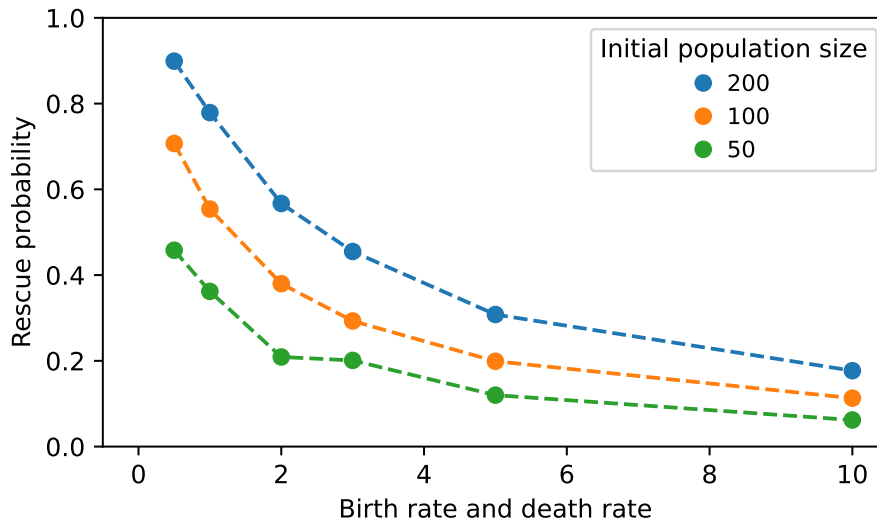


**Figure 4 Probability of evolutionary rescue.** First parental populations with higher turnover as characterized by higher levels of equal birth and death rate are less likely to successfully adapt and escape extinction. Rescue probability is here defined as the fraction of non-extinct replicate populations after  $t_f = 500t = 500$ , which allows non-extinct populations to move far into trait space regions of high net growth rate and high survival probability (see for example Fig. 2). Simulations are started from ~~identical the initial conditions and parental population size  $N_0$  using~~ 1000 replicates.

263 In those replicates where the population does not go extinct, we see that the ensemble average popula-  
 264 tion size tracks the effective carrying capacity  $N^*$  of the ensemble and approaches the carrying capacity  
 265  $K$  in a sigmoidal fashion (Fig. 5). The corresponding ensemble trajectory of untreated trait adaptation  
 266 describes a circular shape in trait space, as predicted by both the survival probability fitness gradient  
 267 and, if the population size equals the effective carrying capacity, the net growth fitness gradient.

### 268 3.2. Trajectories of adaptation in treated populations

269 For both plausible fitness gradients we can construct geometrical hypotheses about the effect of treat-  
 270 ment on the adaptation trajectory. Visualizing the fitness isoclines (the lines of equal fitness) in trait  
 271 space as the rectangular bases for the fitness gradient vectors helps to work out this effect (Fig. 6). We  
 272 consider ~~different kinds of treatment~~ treatment types that either target the population size directly,  
 273 or indirectly by additively shifting the traits of the cells which subsequently decreases population size.  
 274 Both the direct as well as the indirect effect on population size induce a density-mediated ~~change in the~~  
 275 ~~predicted adaptation direction of the~~ rotation in the net growth fitness ~~component, which becomes less~~

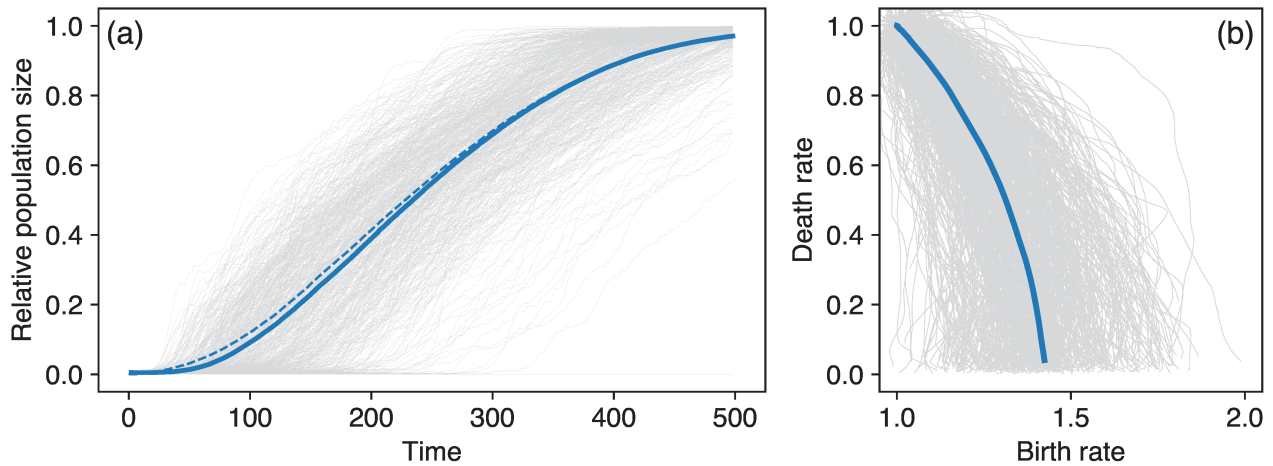


**Figure 5 Ensemble population size dynamics and trait trajectories without treatment.**

(a) The population size  $N$  increases to the carrying capacity  $K$  in those replicate populations (light grey) that do not go extinct. The solid blue line represents the ensemble average of the surviving populations, the dashed blue line is the effective carrying capacity  $N^*$  of these replicates. (b) The trait trajectories (light grey) of all replicates on average describe a circular shape (blue line). To characterize the ensemble, we consider 1000 replicates of the simulation in Fig. 2.

276 ~~vertical and gains a larger birth rate component~~ isoclines (Fig. 6a). This causes a less vertical predicted  
 277 adaptation direction with a larger birth rate component from the net growth fitness component. The  
 278 trait-affecting treatment types temporally displace the population in trait space but have no direct  
 279 effect on the net growth fitness component due to the parallel fitness isoclines (Fig. 6b). Similarly,  
 280 the survival probability fitness component is independent of population size and thus not affected by  
 281 density changes (Fig. 6c). However, ~~the~~ when the population is displaced in trait space the circular  
 282 shape of the survival probability fitness component changes the predicted adaptation direction to be  
 283 come less vertical under trait-affecting treatment (Fig. 6d). Thus, we hypothesize that both treatment  
 284 types would drive less vertical adaptation trajectories.

285 We investigate the effect of treatment on the adaptation trajectory by periodically applying the dif-  
 286 ferent treatment types on populations that grow from small population sizes and ascend the fitness  
 287 gradient (Fig. 7). If the replicate populations escape extinction, they increase in population size and  
 288 reach the carrying capacity  $K$ . The density-affecting treatment type reduces the population size of  
 289 each lineage by a bottleneck factor  $f$ . This decreases competition and allows surviving lineages to



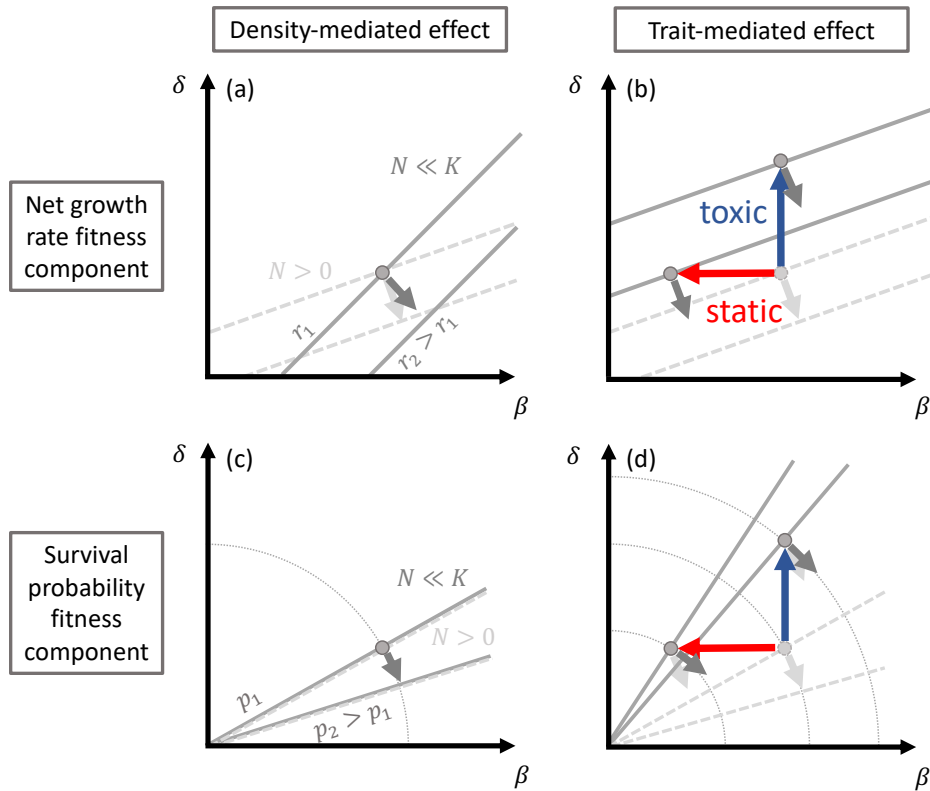


**Figure 6 Density-mediated and trait-mediated treatment effects predict less vertical trait adaptation trajectories.** The fitness isoclines (contours of equal fitness in trait space) are by definition perpendicular to the fitness gradient vectors for a given point in trait space. Fitness isoclines in the absence of treatment are depicted by dashed grey lines, fitness isoclines affected by treatment are shown as solid, dark grey lines. Similarly, realized trait combinations that include the effect of treatment are shown by dark grey points. They deviate from their light grey, untreated counterparts in the case of trait-affecting treatment. Potential changes in the adaptation direction are indicated by a difference between untreated (light grey) and treated (dark grey) fitness gradient vectors, and corresponding fitness isoclines with different angles relative to the axes.

290 achieve higher net growth rate. This competitive release causes the population size to recover to  
 291 higher levels after the first treatments than in the untreated control (Fig. 7a). However, newly estab-  
 292 lished, fitter lineages are especially prone to extinction when the bottleneck treatment reduces lineage  
 293 sizes to small fractions, which limits the exploration of trait space and hinders a rapid adaptation  
 294 towards faster net growth rates and higher survival probabilities. Therefore, the populations that  
 295 undergo stronger bottleneck treatments approach the carrying capacity slower and have shorter trait  
 296 trajectories (Fig. 7a,b). The trait-affecting treatment types also show the competitive release pattern  
 297 of recovery to population sizes higher than the untreated control. Here, the population sizes repeatedly

298 recover to higher values after treatment and the carrying capacity is approached faster than in the un-  
299 treated control (Fig. 7c,d). Similar to the untreated population size time series, also under treatment  
300 the population size is tracking the effective carrying capacity  $N^*$ . We find that the trait trajectories of  
301 treated populations deviate from the untreated controls as predicted from our geometrical hypotheses  
302 (Fig. 6). We observe that the deviations are caused by more horizontal adaptation steps right after  
303 the density-affecting treatment or during the trait-affecting treatment (Figs. S7, S8). This results in  
304 longer adaptation trajectories that are elongated towards higher birth rates. The traits change in a  
305 step-wise pattern over time for the density-affecting treatment, with large adaptive steps immediately  
306 after the treatment time points (Fig. 8a). Trait-affecting treatment increases the rate of trait change  
307 which results in a ramp-like pattern of the traits over time Fig. 8b).

308 We find that the dynamics of those trait-affecting treatment types that contain toxic components are  
309 similar both in the population size and the trait dynamics. The purely static treatment, however, differs  
310 considerably. As the population size approaches the carrying capacity, the effect of the static treat-  
311 ment is reduced as its net growth reduction is density dependent and proportional to  $1 - N/K$  (Eq. 1).  
312 This manifests in decreasing density reductions during treatment phases (Fig. 7c). Accordingly, after  
313 similar initial trajectories, the adaptation trajectory under purely static treatment later deviates from  
314 the adaptation trajectories for the other treatment types that contain also density-independent toxic  
315 components (Fig. 7d). We observe similar patterns also in the deterministic description of the adap-  
316 tive process using a quantitative genetics approach where we explicitly specify the gradient of trait  
317 adaptation (Eq. 3, Figs. S9, S10).

318 These fundamental effects of different treatment types on population dynamics and trait adaptation  
319 trajectory translate to treatment efficiency and the possibility for the populations to escape the treat-  
320 ment, i.e. evolve treatment tolerance. In our model and for the chosen parameters, approximately half  
321 of the replicates go extinct without any treatment due to stochastic extinction in the initial phases  
322 of adaptation. This pattern is caused by the initially equal birth and death rates. Equal birth and  
323 death rates imply zero net growth and thus inevitable extinction due to stochastic population size

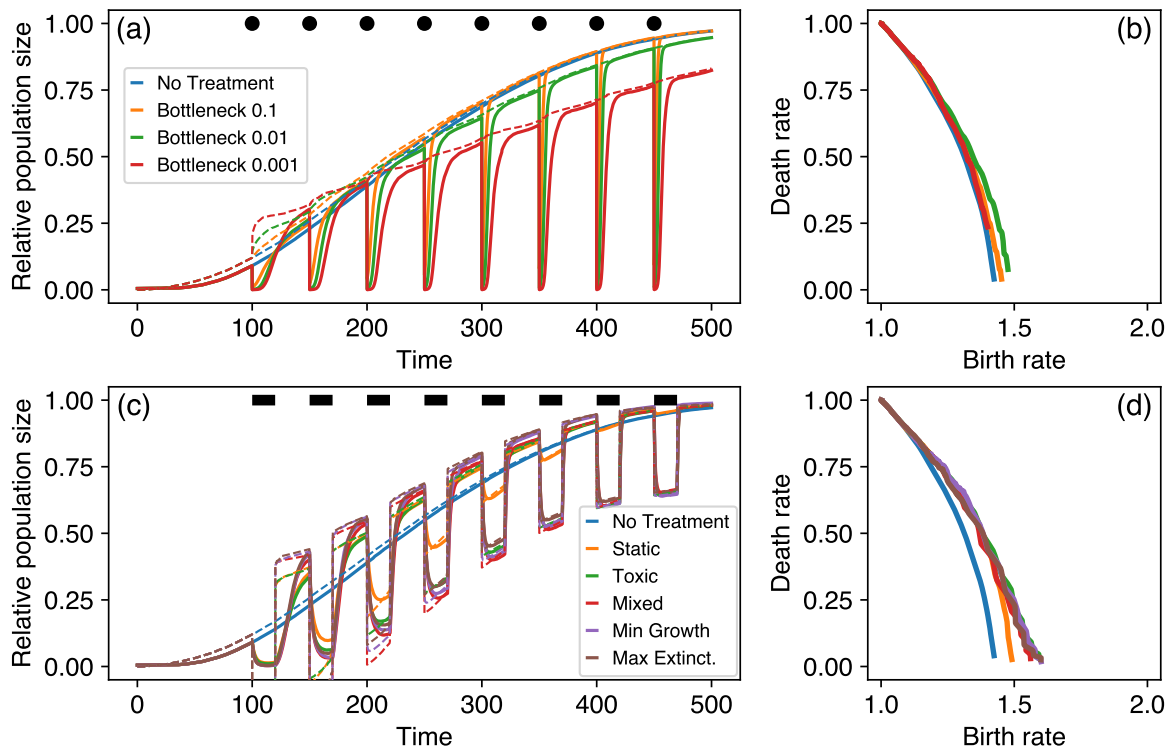


**Figure 7 Ensemble population size dynamics and trait trajectories under treatment.** (a) Density-affecting treatment applies regular bottlenecks and instantaneously decreases the population size of each lineage to a small fraction at time points indicated by the black points. The treatment strength is varied by decreasing the remaining fraction of each lineage after treatment (different colors). The population size dynamics track the effective carrying capacity (Eq. 4, dashed lines). (b) The density-affecting treatment affects the ensemble trait trajectory by triggering sudden trait changes. (c) Trait-affecting treatment types result in prolonged phases of reduced population size (indicated by the black bars). Again, the dashed lines depict the effective carrying capacity dynamics. (d) The ensemble average trait trajectories under trait-affecting treatment deviate from the no treatment reference and reach higher birth rates. Exemplary population size time series and trait trajectories for bottleneck, static and toxic treatment are shown in Figs. S4-S6. As before we performed 1000 replicate simulations and computed ensemble averages from the surviving replicates.

324 fluctuations. The adapting populations depart from this. Applying treatment increases the fraction  
 325 of extinct replicates, which we use as a measure to quantify the treatment success rate (Fig. 9). As  
 326 expected, a higher treatment strength that removes a larger proportion of cells per lineage increases  
 327 the success rate of the density-affecting treatment type. Among the trait-affecting treatment types,  
 328 pure static and toxic treatments achieve a similar success rate. Interestingly, combining static and  
 329 toxic treatment components results in a considerably higher success rate. Here, the success rate of  
 330 treatment types that counter either the net growth fitness gradient or the survival probability fitness

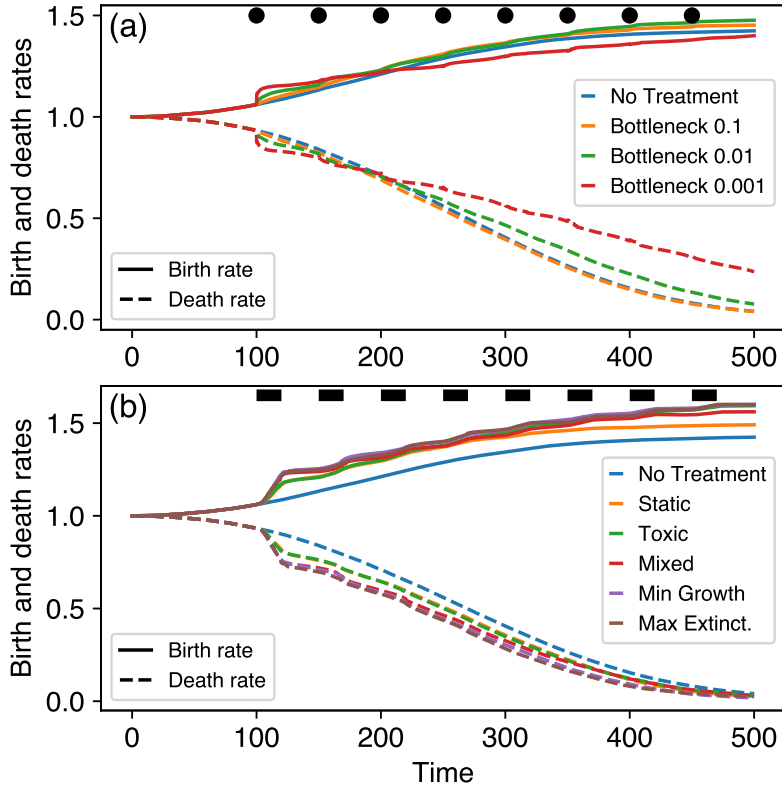


**Figure 8 Trait dynamics under treatment depict the speed of adaptation.** (a) Density-affecting treatment causes short spikes in adaptation speed that manifest in step-wise changes of the ensemble trait average. (b) Trait-affecting treatment temporarily accelerates the changes in ensemble trait averages leading to ramp-like trait changes. The different colors refer to the treatment types, the solid and dashed lines represent birth and death rates, respectively.

331 gradient is slightly higher than the 'Mixed' treatment type that non-adaptively blends the static and  
 332 toxic components in equal proportion.

333 An interesting pattern emerges for the overall number of lineages that are eventually created during the  
 334 adaptation from one parental lineage, which relates to the evolutionary potential of the population.

335 We find that treatments that particularly increase mortality while not decreasing birth rates lead  
 336 to a higher number of created lineages. The higher mortality decreases the density limitation of

337 birth rates, which enables high net birth rates and accordingly high mutation rates. Particularly the  
 338 stronger density-affecting treatments and the purely toxic treatment result in the creation of more

339 mutant lineages. Whether these lineages are expanding successfully and thus shift the population  
 340 average trait combination depends on the survival of the newly created lineages. Accordingly, we

341 find a reduced exploration for the strongest density-affecting treatment measured by the distance  
342 between the first parental trait combination and the population average trait combination at the end  
343 of our simulations. For the trait-affecting treatment types, we find an opposite correlation. Here,  
344 more lineages also enable a further trait space exploration. Newly created lineages are in general more  
345 endangered by extinction than established lineages, simply because of their smaller cell numbers, which  
346 makes a stochastic crossing of the extinction boundary more likely. During bottleneck treatment the  
347 relative effects of treatment on the extinction risk for newly created, fitter lineages versus established,  
348 less fit lineages are equal, whereas the absolute effects are different as it is more likely for small lineages  
349 to be driven to population sizes below a single cell. During trait-affecting treatment, the relative effect  
350 of treatment is smaller for smaller, but fitter lineages than for established, less fit lineages, whereas  
351 the absolute effects are equal. This may explain the observed differences in the correlation of number  
352 of lineages and evolved trait distance. It is interesting to note that treatments with higher success rate  
353 were also found to induce faster trait changes (Fig. 8), pointing out a potential trade-off of treatment  
354 success versus driving tolerance evolution.

### 355 **3.3. Which fitness component is more important?**

356 We found that treatment types that counter the potential fitness gradients achieve the highest success  
357 rates. However, we have not conclusively answered whether the net growth fitness gradient or the  
358 survival probability fitness gradient are more decisive for the eco-evolutionary dynamics in our model.  
359 To gather more evidence on this, we sampled the initial adaptation direction from different initial trait  
360 combinations to visualize the realized fitness gradient that acts on the adapting populations in trait  
361 space (Fig. S11). We indeed find that the realized fitness gradients are non-parallel in trait space,  
362 indicating that for larger birth rates and smaller death rates adaptation is driven by decreasing death  
363 rate, and increasing birth rate becomes less important. The visual similarity of this pattern to the  
364 survival probability fitness gradient hints at a larger importance of the survival probability fitness  
365 gradient at first glance. However, also the net growth rate becomes larger for larger birth rates and

366 smaller death rates, which speeds up the population size increase during the short observation window  
367 of initial adaptation. Because of the density-dependence, these larger population sizes turn the net  
368 growth fitness gradient to be more vertical (see Fig. 3a). Also, we observe that the initial adaptation  
369 direction is largely parallel along the diagonals in trait space, which correspond to the net growth  
370 fitness isoclines for small population sizes, which favours the net growth fitness gradient to be more  
371 important.

372 To investigate whether the differences in initial adaptation direction are indeed caused by the density-  
373 dependence of the net growth fitness gradient, we again investigated the initial steps of adaptation  
374 with parameters that minimize the density change within our observation window. We decreased the  
375 initial population size and time span and increased the carrying capacity and find that the adaptation  
376 direction indeed becomes more horizontal, indicating a larger importance of the net growth fitness  
377 gradient than the survival probability fitness gradient. If the survival probability fitness gradient  
378 would be predominantly driving the adaptation, we would expect that the initial steps of adaptation  
379 change along the net growth fitness isoclines (except for the diagonal passing through the origin) and  
380 we would not expect a density dependence.

381 In the deterministic model (Eq. 3), we are explicitly prescribing the fitness measure that determines  
382 the direction of trait adaptation. If we choose the net growth as the determining fitness measure  
383 we find trait trajectories that change with treatment and reproduce the trajectories obtained from  
384 simulations (Fig. S9). However, if we set the survival probability as the determining fitness measure  
385 in the deterministic model the trait trajectories under density-affecting treatment do not deviate from  
386 the trajectories without treatment, thus contrasting the observation in the simulations (Fig. S10).  
387 Therefore, more evidence points towards net growth rate maximization as the determinant of trait space  
388 adaptation trajectories in our simulations, even though we cannot falsify that the survival probability  
389 fitness gradient could also play an important part.

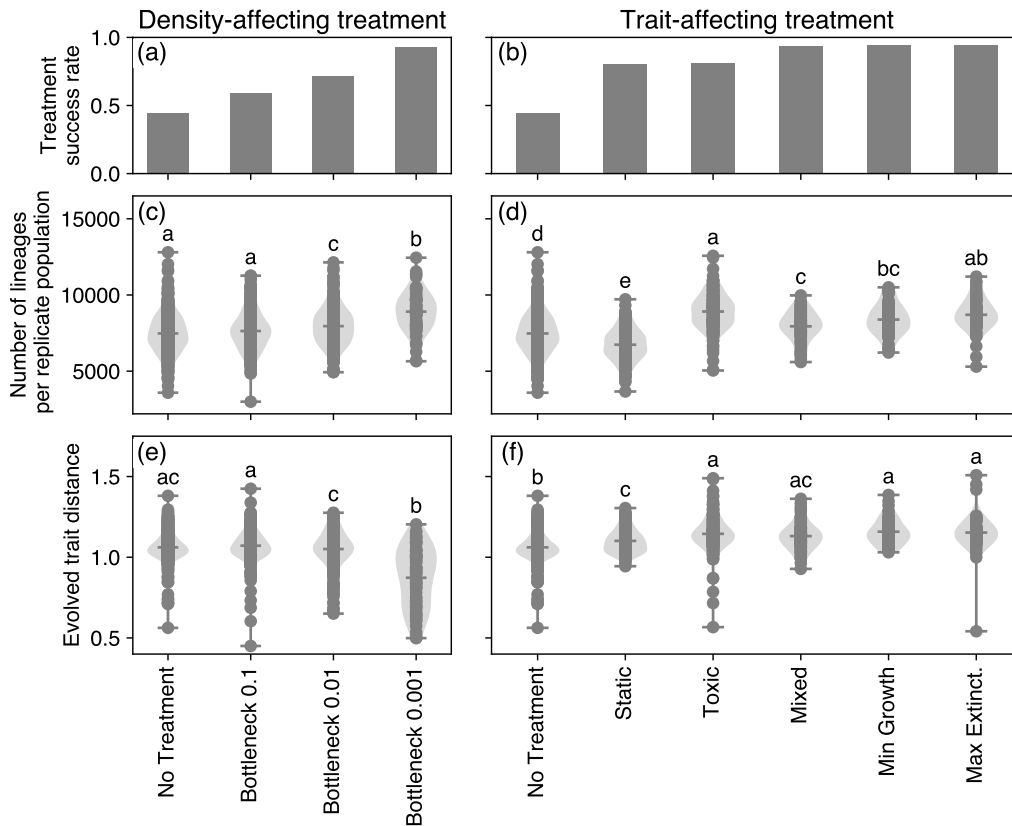


**Figure 9 Treatment effects for density-affecting (left column) and trait-affecting (right column) types.** Panels (a) and (b) show treatment success rate measured as the fraction of extinction among the 1000 replicate populations at  $t = t_f$ . Panels (c) and (d) show the number of lineages that have been created by mutations in each non-extinct replicate population. Panels (e) and (f) show the distance between the first parental trait combination and the last average trait combination of each non-extinct replicate population. In panels (c)-(f), the same lower-case letters above two treatments indicate that the two sets of data points could have been generated from the same underlying distribution. Differing lower-case letters thus indicate differences between treatments. Unique letters indicate treatments that are statistically different from all other treatments. The grouping into statistically different groups was determined using the Tukey’s HSD implementation from the statsmodels module (v0.13.0) in Python 3.8 and assigned with the pairwisecomp\_letters function written by Philip Kirk (<https://github.com/PhilPlantMan/Python-pairwise-comparison-letter-generator>). A treatment can be part of multiple groups by being indifferent to each one of them and thus receive multiple letters.

## 390 4. Discussion

391 During the onset of cancer establishment and the spread of pathogens from a chronic infection, popu-  
392 lations of small size have to break with homoeostatic regulations that aim to prevent their expansion.  
393 Adaptation by trait evolution allows them to climb up the fitness landscape and eventually escape  
394 stochastic extinction, that would be unavoidable without adaptation. In this study, we reduced the  
395 complexity of cancer cells and pathogenic bacteria to the three basic processes of birth, death and  
396 mutation, and investigated i) the shape of the fitness landscape, ii) the adaptive trajectories of trait  
397 evolution and iii) how these trajectories are altered by treatment. We proposed net growth rate and  
398 survival probability as possible fitness measures that are increased by evolution. We found that both  
399 of these measures motivate a circular adaptive trajectory in the trait space spanned by birth rate and  
400 death rate [\(Fig. 3\)](#). Indeed, this circular trajectory is recovered in stochastic simulations [\(Fig. 5\)](#) and  
401 altered by treatment in agreement with geometrically derived hypotheses [\(Figs. 6, 7\)](#). [Interestingly,](#)  
402 [we find that adaptive steps that maximize net growth rate or survival probability always have parallel](#)  
403 [components, indicating no strong conflict between optimizing for either of the two plausible fitness](#)  
404 [measures.](#)

405 In this study, we deliberately chose parameters that would result in occasional extinction of replicate  
406 populations to represent the stochastic nature of the establishment of cancer or bacterial infections  
407 and the stochasticity in treatment response (Coates et al., 2018; Alexander and MacLean, 2020).  
408 This results in a setting where evolutionary rescue is required for the populations to prevent their  
409 extinction. In our model, the population dynamics are captured by the dynamics of the effective  
410 carrying capacity which is the target population size that the total population size is tracking over  
411 time. If birth rates and death rates are equal, the effective carrying capacity is zero and the population  
412 goes extinct deterministically. The effective carrying capacity becomes positive only if the death rate  
413 becomes smaller than the birth rate by trait adaptation, thus also increasing the chances of population  
414 establishment.



415 The shape of the fitness landscape has important implications for the effect of turnover on the rescue  
 416 probability in the cancer or bacterial cell population, which we can again address using geometrical  
 417 arguments of the fitness isoclines. A faster turnover implies that birth rates and death rates of the  
 418 associated cells are higher. This puts fast-turnover cells in the upper right corner of our birth-death  
 419 trait space, and slow-turnover quasi-dormant cells in the lower left. The circular fitness gradient vector  
 420 field of survival probability implies radial fitness isoclines, resulting in an increasing distance between  
 421 isoclines going from slow to fast turnover. Therefore, the same adaptation step in trait space gains  
 422 a smaller increase in the survival probability of fast-turnover cells than in slow-turnover cells. This  
 423 implies that evolutionary rescue is less likely in populations of fast-turnover cells, which we indeed find  
 424 when comparing the fractions of surviving replicates for different initial parental trait combinations  
 425 of equal birth and death rates. Interestingly, Kuosmanen et al. (2022) come to similar conclusions  
 426 in a slightly different model. Importantly, this pattern can be affected by the assumptions on the  
 427 mutational effect sizes. Throughout this study we have assumed additive mutational effects where  
 428 the adaptation step sizes are independent of the trait values. If, however, the mutational effects were  
 429 dependent on the trait values, as for example in the case of multiplicative mutational effects (Fig. S3),  
 430 this pattern will change. Accordingly, we find that multiplicative mutational effects compensate for the  
 431 increasing distance of radial fitness isoclines at larger birth and death rates and the rescue probability  
 432 becomes largely independent of turnover.

433 Besides the shape of the fitness landscape, the declining rescue probability for faster turnover may  
 434 also be explained with the higher rate at which the initial parental lineage declines. At equal birth  
 435 and death rate, the logistic competition term results in a deterministic rate of population decline of  
 436  $-\beta_0 N_0^2/K - \beta_0 N_0(t)^2/K$  in our model, which increases proportional to the birth rate. As this initial  
 437 parental lineage is the source from which offspring lineages are created, a faster decline shortens the  
 438 time window during which fitter lineages can emerge and impedes the race against extinction (Orr  
 439 and Unckless, 2008, 2014; Carlson et al., 2014; Marrec and Bitbol, 2020a). On the other hand, in fast-  
 440 turnover cells mutations occur more frequently because of the higher birth rate, which could speed

441 up the ascend of the survival probability fitness gradient. Our results show that the higher realized  
442 mutation rate cannot ~~counteract~~ compensate for the two detrimental effects of faster turnover firstly  
443 requiring larger trait changes for the same gain in survival probability and secondly leading to a faster  
444 decline in the initial parental lineage.

445 Cancer cell populations as well as bacterial biofilms in chronic infections possess a considerable geno-  
446 typic and phenotypic heterogeneity (Caiado et al., 2016; Gay et al., 2016; Winstanley et al., 2016; Dhar  
447 et al., 2016). In a heterogeneous population consisting of lineages with different turnover but individ-  
448 ually equal birth and death rates our results imply that those lineages with smaller turnover would  
449 persist longer. Evolutionary rescue would thus be achieved on average from those lower-turnover  
450 lineages hinting at a selective advantage of low turnover in heterogeneous populations in challeng-  
451 ing environments, which ~~is supported by~~ may explain the therapeutic challenges posed by dormant  
452 subpopulations both in cancer (Yeh and Ramaswamy, 2015; Ammerpohl et al., 2017) and bacterial  
453 infections (Wood et al., 2013). Birth (proliferation) and death (apoptosis) are partly interlinked in  
454 their regulation (Alenzi, 2004) and measuring their rates in eukaryotic cells is possible in vitro and  
455 in vivo (Lyons and Parish, 1994). Different tissue types were shown to have intrinsically different  
456 turnover rates (Sender and Milo, 2021) and turnover can be altered experimentally (Casey et al.,  
457 2007). Several studies reported a positive correlation of proliferation and apoptosis in breast cancer  
458 (de Jong et al., 2000; Liu et al., 2001; Archer et al., 2003), which suggests a positive correlation of  
459 birth and death rate. Prognosis was found to be worse for higher birth rate (Liu et al., 2001). Our  
460 model proposes that such aggressive, quickly growing tumours with a high cell death rate are actually  
461 less likely to persist than tumours with lower turnover as the probability for evolutionary rescue de-  
462 creases with turnover. This apparent dichotomy indicates that the evolutionary rescue probability of a  
463 tumour not necessarily translates into its prognosis and that clinically we tend to only observe the few  
464 high-turnover tumours that have managed to escape homeostatic regulation, while remaining blind to  
465 those with lower turnover. Also in the context of chronic bacterial infections there exist methods to  
466 assess turnover in bacterial pathogen populations in vitro (Stewart et al., 2005; Wang et al., 2010).

467 They are currently developed for in vivo settings (Myhrvold et al., 2015; Mahmutovic et al., 2021)  
468 and will soon elucidate the different intrinsic birth and death rates of bacterial strains and species,  
469 sometimes even working out spatial parameter heterogeneity within the body (Gillman et al., 2021).  
470 It will be interesting to see whether indeed lower-turnover regions of the birth-death trait-space are  
471 found to be more populated and whether trait evolution indeed proceeds along the circular trajectory  
472 predicted by our model.

473 Fitness landscapes of mutational changes can be constructed from data (Watson et al., 2020) and used  
474 in treatment via evolutionary steering (Nichol et al., 2015; Acar et al., 2020). Accounting for their  
475 temporal variability (e.g. under the effect of treatment), then sometimes referring to them as fitness  
476 seascapes, has important consequences for the understanding of adaptation, such as resistance evolution  
477 (Lässig et al., 2017; King et al., 2022). For example, Hemez et al. (2020) found in a simulation study  
478 that the drug mode of action (bacteriostatic vs. bactericidal) was changing the shape of the fitness  
479 landscape. In line with this, we have found that both density-affecting and trait-affecting treatment  
480 types alter trait adaptation trajectories. The density-mediated effect of treatment rotates the fitness  
481 landscape, the trait-mediated treatment effect relocates populations to other trait combinations in  
482 trait space. Both of these effects increase the birth rate component of adaptive steps which causes  
483 treated trait adaptation trajectories to depart from untreated trajectories.

484 We found profound patterns of competitive release in the population dynamics of successfully adapting  
485 populations (Wargo et al., 2007). In the off-treatment phases, the treated and non-extinct populations  
486 quickly recover to population sizes up to twice as large as in the untreated reference. The competitive  
487 release is particularly strong for the trait-affecting treatment types. This is in line with the fact that  
488 the trait-affecting treatment exerts a higher relative penalty on less fit lineages than on fitter lineages  
489 as we assumed additive treatment effects and thus the mortality during treatment is higher for less  
490 fit lineages. In our model the effect of static drugs decreases as the population size approaches the  
491 carrying capacity where the effective birth rate tends to zero even without treatment and thus can not  
492 be reduced further by treatment. Contrastingly, the sustained mortality exerted by toxic treatment

493 also at population sizes close to the carrying capacity leads to a continuing competitive release. This  
494 creates additional transient phases of population recovery after treatment phases during which birth  
495 and mutation rates are high, resulting in faster adaptation. This potentially negative effect of toxic  
496 treatment is in agreement with findings by [Anttila et al. \(2019\)](#) and [Marrec and Bitbol \(2020b\)](#) and  
497 similar to the paradoxical negative effects of apoptosis during tumour development ([Labi and Erlacher,](#)  
498 [2015](#)). This finding also resonates with the rationale behind tumour containment treatment strategies  
499 that aim at preserving sensitive subpopulations as competitors, and thus suppressors, of resistant  
500 subpopulations ([Gatenby et al., 2009](#); [Viossat and Noble, 2021](#)).

501 Time-resolved surveillance of treatment responses in both cancer and bacterial infections promises to  
502 prevent resistance evolution, but is technically and practically challenging. Accordingly, the quest for  
503 personalized, resistance-proof treatment approaches remains one to be fulfilled. In a recent paper, we  
504 found that increasing the temporal frequency of surveillance has diminishing returns and also more  
505 coarse-grained surveillance patterns could achieve large treatment improvements ([Raatz et al., 2021](#)).

506 Interestingly, in the present study we find that the mixed treatment which is agnostic to real-time  
507 information performs almost as good as the treatment types that counter the fitness gradient and thus  
508 necessitate ongoing temporal information on the population trait average. This again suggests that  
509 large treatment improvements can be achieved already with low surveillance effort. The high efficiency  
510 of static and toxic treatment combinations is in agreement with theoretical predictions ([Lorz et al.,](#)  
511 [2013](#)) and recently explored approaches in cancer treatment, such as the combination of navitoclax,  
512 a drug that increases the apoptosis rate, and cytostatics such as gemcitabine or brentuximab which  
513 decrease the birth rate ([Cleary et al., 2014](#); [Ju et al., 2016](#); [Montero and Letai, 2018](#)). Also in bacteria,  
514 recent findings suggest that a combination of bacteriostatic drugs (or nutrient deprivation) and bacte-  
515 ricidal drugs indeed increase the extinction probability of bacterial microcolonies ([Coates et al., 2018](#)).

516 However, awareness of the mechanisms of action and the interactive effects is essential, as treatment  
517 efficiency can also be reduced in combination treatments, for example if the bactericidal drug relies  
518 on cell growth that is reduced by the bacteriostatic drug ([Bollenbach et al., 2009](#); [Bollenbach, 2015](#);

519 [Coates et al., 2018](#)). An additional advantage of combination therapies that was not considered in  
520 our study is that resistance is less likely to evolve in parallel against two independently active drugs.  
521 Consequently, drug interactions have important consequences not only for treatment efficiency but also  
522 for resistance evolution ([Roemhild et al., 2018](#); [Roemhild and Schulenburg, 2019](#); [Batra et al., 2021](#);  
523 [Jaaks et al., 2022](#)).

524 In this study, we have abstracted from the physiological details of different adaptation pathways in  
525 evolving cell populations and the molecular mechanisms of the drugs used to counter these adapta-  
526 tions. By mapping these details to traits with clear eco-evolutionary consequences we achieved an  
527 understanding of the adaptation dynamics, identified relevant fitness components and showed the high  
528 efficiency of trait-aware treatment strategies. Current experimental and diagnostic advancements en-  
529 able the identification of traits, such as birth and death rates, at realistic scales to allow for a translation  
530 between mechanistic models such as ours and experimental and clinical observations. This will further  
531 the understanding of the eco-evolutionary mechanisms at play in the dynamics of cancer and bacterial  
532 infections and sprout improved, personalized and adaptive treatment strategies.

### 533 **Data, script and code availability**

534 The code to reproduce all figures has been deposited at <https://doi.org/10.5281/zenodo.6656842>.

535 The simulation data is available at <https://doi.org/10.5281/zenodo.6656847>.

### 536 **Funding**

537 [We acknowledge funding by Deutsche Forschungsgemeinschaft through the Research Training Group](#)

538 [“Translational Evolutionary Research” \(TransEvo\) \(Project number 400993799,](#)

539 <https://gepris.dfg.de/gepris/projekt/400993799>).

540 **Conflict of interest disclosure**

541 The authors declare they have no conflict of interest relating to the content of this article.

542 **Acknowledgements**

543 We thank Hildegard Uecker for discussions and advice on the probability of evolutionary rescue. We  
544 are grateful for biological insights into the birth and death of bacteria from Javier Lopez Garrido and  
545 Alan Derman and for discussions related to birth and death of cancer cells with Susanne Sebens and  
546 Lisa-Marie Philipp.

## References

- P. A. Abrams and H. Matsuda. Prey adaptation as a cause of predator-prey cycles. *Evolution*, 51(6):1742–1750, 1997.
- A. Acar, D. Nichol, J. Fernandez-Mateos, G. D. Cresswell, I. Barozzi, S. P. Hong, N. Trahearn, I. Spiteri, M. Stubbs, R. Burke, A. Stewart, G. Caravagna, B. Werner, G. Vlachogiannis, C. C. Maley, L. Magnani, N. Valeri, U. Banerji, and A. Sottoriva. Exploiting evolutionary steering to induce collateral drug sensitivity in cancer. *Nature Communications*, 11(1):1923, 2020.
- F. Alenzi. Links between apoptosis, proliferation and the cell cycle. *British Journal of Biomedical Science*, 61(2):99–102, 2004. doi: 10.1080/09674845.2004.11732652.
- H. K. Alexander and R. C. MacLean. Stochastic bacterial population dynamics restrict the establishment of antibiotic resistance from single cells. *Proceedings of the National Academy of Sciences*, 117(32):19455–19464, 2020. doi: 10.1073/pnas.1919672117.
- H. K. Alexander, G. Martin, O. Y. Martin, and S. Bonhoeffer. Evolutionary rescue: linking theory for conservation and medicine. *Evolutionary Applications*, 7(10):1161–1179, Dec. 2014. doi: 10.1111/eva.12221.
- O. Ammerpohl, K. Hattermann, J. Held-Feindt, C. Röcken, H. Schäfer, C. Schem, D. Schewe, H. Schulenburg, S. Sebens, M. Synowitz, S. Tiwari, A. Traulsen, A. Trauzold, T. Valerius, and D. Wesch. *Dormancy: An Evolutionary Key Phenomenon in Cancer Development*, chapter 20, pages 235–242. Ecology and Evolution of Cancer, 2017.
- J. V. Anttila, M. Shubin, J. Cairns, F. Borse, Q. Guo, T. Mononen, I. Vázquez-García, O. Pulkkinen, and V. Mustonen. Contrasting the impact of cytotoxic and cytostatic drug therapies on tumour progression. *PLoS Computational Biology*, 15(11):e1007493, Nov. 2019. doi: 10.1371/journal.pcbi.1007493.
- C. D. Archer, M. Parton, I. E. Smith, P. A. Ellis, J. Salter, S. Ashley, G. Gui, N. Sacks, S. R. Ebbs, W. Allum, N. Nasiri, and M. Dowsett. Early changes in apoptosis and proliferation following primary chemotherapy for breast cancer. *British Journal of Cancer*, 89(6):1035–1041, 2003. doi: 10.1038/sj.bjc.6601173.
- D. Basanta and A. R. Anderson. Homeostasis back and forth: An ecoevolutionary perspective of cancer. *Cold Spring Harbor Perspectives in Medicine*, 7(9):1–20, 2017. doi: 10.1101/cshperspect.a028332.
- D. Basanta and A. R. A. Anderson. Exploiting ecological principles to better understand cancer progression and treatment. *Interface Focus*, 3(4):20130020–20130020, 2013. doi: 10.1098/rsfs.2013.0020.
- A. Batra, R. Roemhild, E. Rousseau, S. Franzenburg, S. Niemann, and H. Schulenburg. High potency of sequential therapy with only beta-lactam antibiotics. *eLife*, 10:e68876, 2021.
- D. K. Biswas, Q. Shi, S. Baily, I. Strickland, S. Ghosh, A. B. Pardee, and J. D. Iglehart. NF- $\kappa$ B activation in human breast cancer specimens and its role in cell proliferation and apoptosis. *Proceedings of the National Academy of Sciences*, 101(27):10137–10142, July 2004. doi: 10.1073/pnas.0403621101.
- T. Bollenbach. Antimicrobial interactions: mechanisms and implications for drug discovery and resistance evolution. *Current Opinion in Microbiology*, 27:1–9, Oct. 2015. doi: 10.1016/j.mib.2015.05.008.

- T. Bollenbach, S. Quan, R. Chait, and R. Kishony. Nonoptimal Microbial Response to Antibiotics Underlies Suppressive Drug Interactions. *Cell*, 139(4):707–718, Nov. 2009. doi: 10.1016/j.cell.2009.10.025.
- A. Both, J. Huang, M. Qi, C. Lausmann, S. Weißelberg, H. Büttner, S. Lezius, A. V. Failla, M. Christner, M. Stegger, T. Gehrke, S. Baig, M. Citak, M. Alawi, M. Aepfelbacher, and H. Rohde. Distinct clonal lineages and within-host diversification shape invasive *Staphylococcus epidermidis* populations. *PLoS Pathogens*, 17(2):e1009304, Feb. 2021. doi: 10.1371/journal.ppat.1009304.
- F. Caiado, B. Silva-Santos, and H. Norell. Intra-tumour heterogeneity – going beyond genetics. *FEBS Journal*, 283(12):2245–2258, 2016.
- S. M. Carlson, C. J. Cunningham, and P. A. Westley. Evolutionary rescue in a changing world. *Trends in Ecology and Evolution*, 29(9):521–530, 2014. doi: 10.1016/j.tree.2014.06.005.
- T. Casey, T. Mulvey, T. Patnode, A. Dean, E. Zakrzewska, and K. Plaut. Mammary epithelial cells treated concurrently with  $\text{tgf-}\alpha$  and  $\text{tgf-}\beta$  exhibit enhanced proliferation and death. *Experimental Biology and Medicine*, 232(8):1027–1040, 2007.
- J. M. Cleary, C. M. S. R. Lima, H. I. Hurwitz, A. J. Montero, C. Franklin, J. Yang, A. Graham, T. Busman, M. Mabry, K. Holen, G. I. Shapiro, and H. Uronis. A phase I clinical trial of navitoclax, a targeted high-affinity Bcl-2 family inhibitor, in combination with gemcitabine in patients with solid tumors. *Investigational New Drugs*, 32(5):937–945, 2014. doi: 10.1007/s10637-014-0110-9.
- J. Coates, B. R. Park, D. Le, E. Şimşek, W. Chaudhry, and M. Kim. Antibiotic-induced population fluctuations and stochastic clearance of bacteria. *eLife*, 7:e32976, Mar. 2018. doi: 10.7554/eLife.32976.
- C. E. Cox and F. Hinman. Experiments with Induced Bacteriuria, Vesical Emptying and Bacterial Growth on the Mechanism of Bladder Defense to Infection. *Journal of Urology*, 86(6):739–748, Dec. 1961. doi: 10.1016/S0022-5347(17)65257-1.
- M. J. Culyba and D. V. Tyne. Bacterial evolution during human infection: Adapt and live or adapt and die. *PLoS Pathogens*, 17(9):e1009872, Sept. 2021. doi: 10.1371/journal.ppat.1009872.
- J. S. de Jong, P. J. v. Diest, and J. P. A. Baak. Number of apoptotic cells as a prognostic marker in invasive breast cancer. *British Journal of Cancer*, 82(2):368–373, 2000. doi: 10.1054/bjoc.1999.0928.
- N. Dhar, J. McKinney, and G. Manina. Phenotypic Heterogeneity in *Mycobacterium tuberculosis*. *Microbiology Spectrum*, 4(6):4.6.10, 2016. doi: 10.1128/microbiolspec.TBTB2-0021-2016.
- M. Doebeli, Y. Ispolatov, and B. Simon. Towards a mechanistic foundation of evolutionary theory. *eLife*, 6:e23804, 2017.
- E. Faure, K. Kwong, and D. Nguyen. *Pseudomonas aeruginosa* in Chronic Lung Infections: How to Adapt Within the Host? *Frontiers in Immunology*, 9:2416, 2018. doi: 10.3389/fimmu.2018.02416.
- A. Frenoy and S. Bonhoeffer. Death and population dynamics affect mutation rate estimates and evolvability under stress in bacteria. *PLOS Biology*, 16(5):e2005056, May 2018. doi: 10.1371/journal.pbio.2005056.
- W. H. Fridman, F. Pagès, C. Sautès-Fridman, and J. Galon. The immune contexture in human tumours: impact on clinical outcome. *Nature Reviews Cancer*, 12(4):298–306, Apr. 2012. doi: 10.1038/nrc3245.



- J. A. Gallaher, J. S. Brown, and A. R. A. Anderson. The impact of proliferation-migration tradeoffs on phenotypic evolution in cancer. *Scientific Reports*, 9(1):2425, 2019. doi: 10.1038/s41598-019-39636-x.
- R. A. Gatenby, A. S. Silva, R. J. Gillies, and B. R. Frieden. Adaptive therapy. *Cancer Research*, 69(11):4894–4903, 2009. ISSN 0008-5472. doi: 10.1158/0008-5472.CAN-08-3658. URL <http://cancerres.aacrjournals.org/content/69/11/4894>.
- L. Gay, A.-M. Baker, and T. A. Graham. Tumour Cell Heterogeneity [version 1; peer review: 5 approved]. *F1000Research*, 5:238, 2016. URL <http://f1000research.com/articles/5-238/v1><https://f1000research.com/articles/5-238/v1>.
- A. N. Gillman, A. Mahmutovic, P. A. z. Wiesch, and S. Abel. The Infectious Dose Shapes *Vibrio cholerae* Within-Host Dynamics. *mSystems*, Dec. 2021. doi: 10.1128/mSystems.00659-21.
- M. Gruber, I. Bozic, I. Leshchiner, D. Livitz, K. Stevenson, L. Rassenti, D. Rosebrock, A. Taylor-Weiner, O. Olive, R. Goyette, S. M. Fernandes, J. Sun, C. Stewart, A. Wong, C. Cibulskis, W. Zhang, J. G. Reiter, J. M. Gerold, J. G. Gribben, K. R. Rai, M. J. Keating, J. R. Brown, D. Neuberg, T. J. Kipps, M. A. Nowak, G. Getz, and C. J. Wu. Growth dynamics in naturally progressing chronic lymphocytic leukaemia. *Nature*, 570(7762):474–479, Jun 2019. doi: 10.1038/s41586-019-1252-x.
- A. R. Hauser, J. Mecsas, and D. T. Moir. Beyond Antibiotics: New Therapeutic Approaches for Bacterial Infections. *Clinical Infectious Diseases*, 63(1):89–95, 2016. doi: 10.1093/cid/ciw200.
- C. Hemez, F. Clarelli, A. C. Palmer, L. Chindelevitch, T. Cohen, and P. A. z. Wiesch. Mechanisms of antibiotic action shape the fitness landscapes of resistance mutations. *bioRxiv*, June 2020. doi: 10.1101/2020.06.01.127571.
- P. Jaaks, E. A. Coker, D. J. Vis, O. Edwards, E. F. Carpenter, S. M. Leto, L. Dwane, F. Sassi, H. Lightfoot, S. Barthorpe, D. van der Meer, W. Yang, A. Beck, T. Mironenko, C. Hall, J. Hall, I. Mali, L. Richardson, C. Tolley, J. Morris, F. Thomas, E. Lleshi, N. Aben, C. H. Benes, A. Bertotti, L. Trusolino, L. Wessels, and M. J. Garnett. Effective drug combinations in breast, colon and pancreatic cancer cells. *Nature*, 603(7899):166–173, 2022. doi: 10.1038/s41586-022-04437-2.
- W. Ju, M. Zhang, K. M. Wilson, M. N. Petrus, R. N. Bamford, X. Zhang, R. Guha, M. Ferrer, C. J. Thomas, and T. A. Waldmann. Augmented efficacy of brentuximab vedotin combined with ruxolitinib and/or Navitoclax in a murine model of human Hodgkin’s lymphoma. *Proceedings of the National Academy of Sciences*, 113(6):1624–1629, Feb. 2016. doi: 10.1073/pnas.1524668113.
- K. M. Kerr and D. Lamb. Actual growth rate and tumour cell proliferation in human pulmonary neoplasms. *British Journal of Cancer*, 50(3):343–349, Sept. 1984. doi: 10.1038/bjc.1984.181.
- E. S. King, J. Pelesko, J. Maltas, S. J. Owen, E. Dolson, and J. G. Scott. Fitness seascapes facilitate the prediction of therapy resistance under time-varying selection. *bioRxiv*, June 2022. doi: 10.1101/2022.06.10.495696. URL <http://biorxiv.org/lookup/doi/10.1101/2022.06.10.495696>.
- A. L. Koch. Death of bacteria in growing culture. *Journal of Bacteriology*, 77(5):623–629, May 1959. doi: 10.1128/jb.77.5.623-629.1959.
- H. Kokko. The stagnation paradox: the ever-improving but (more or less) stationary population fitness. *Proceedings of the Royal Society B: Biological Sciences*, 288(1963):20212145, Nov. 2021. doi: 10.1098/rspb.2021.2145.
- T. Kuosmanen, S. Särkkä, and V. Mustonen. Turnover shapes evolution of birth and death rates. *bioRxiv*, July 2022. doi: 10.1101/2022.07.11.499527.

- V. Labi and M. Erlacher. How cell death shapes cancer. *Cell Death & Disease*, 6(3):e1675–e1675, 2015. doi: 10.1038/cddis.2015.20.
- R. Lande. A quantitative genetic theory of life history evolution. *Ecology*, 63(3):607–615, 1982. ISSN 1939-9170. doi: 10.2307/1936778. URL <http://dx.doi.org/10.2307/1936778>.
- M. Lässig, V. Mustonen, and A. M. Walczak. Predicting evolution. *Nature Ecology & Evolution*, 1(3):0077, Mar. 2017. doi: 10.1038/s41559-017-0077.
- S. Liu, S. M. Edgerton, D. H. Moore, and A. D. Thor. Measures of Cell Turnover (Proliferation and Apoptosis) and Their Association with Survival in Breast Cancer. *Clinical Cancer Research*, 7(6):1716, June 2001.
- J. Lopez and S. W. G. Tait. Mitochondrial apoptosis: killing cancer using the enemy within. *British Journal of Cancer*, 112(6):957–962, Mar. 2015. doi: 10.1038/bjc.2015.85.
- A. Lorz, T. Lorenzi, M. E. Hochberg, J. Clairambault, and B. Perthame. Populational adaptive evolution, chemotherapeutic resistance and multiple anti-cancer therapies. *ESAIM: Mathematical Modelling and Numerical Analysis*, 47(2):377–399, 2013. doi: 10.1051/m2an/2012031.
- A. Lyons and C. R. Parish. Determination of lymphocyte division by flow cytometry. *Journal of Immunological Methods*, 171(1):131–137, May 1994. ISSN 00221759. doi: 10.1016/0022-1759(94)90236-4.
- A. Mahmutovic, A. N. Gillman, S. Lauksund, N.-A. Robson Moe, A. Manzi, M. Storflor, P. Abel zur Wiesch, and S. Abel. RESTAMP – Rate estimates by sequence-tag analysis of microbial populations. *Computational and Structural Biotechnology Journal*, 19:1035–1051, 2021. doi: 10.1016/j.csbj.2021.01.017.
- L. Marrec and A.-F. Bitbol. Adapt or Perish: Evolutionary Rescue in a Gradually Deteriorating Environment. *Genetics*, 216(2):573–583, Oct. 2020a. doi: 10.1534/genetics.120.303624.
- L. Marrec and A.-F. Bitbol. Resist or perish: Fate of a microbial population subjected to a periodic presence of antimicrobial. *PLOS Computational Biology*, 16(4):e1007798, Apr. 2020b. doi: 10.1371/journal.pcbi.1007798.
- G. Masuda, S. Tomioka, H. Uchida, and M. Hasegawa. Bacteriostatic and Bactericidal Activities of Selected Beta-Lactam Antibiotics Studied on Agar Plates. *ANTIMICROB. AGENTS CHEMOTHER.*, 11:7, 1977.
- J. Montero and A. Letai. Why do BCL-2 inhibitors work and where should we use them in the clinic? *Cell Death & Differentiation*, 25(1):56–64, 2018. doi: 10.1038/cdd.2017.183.
- C. Myhrvold, J. W. Kotula, W. M. Hicks, N. J. Conway, and P. A. Silver. A distributed cell division counter reveals growth dynamics in the gut microbiota. *Nature Communications*, 6(1):10039, Nov. 2015. doi: 10.1038/ncomms10039.
- D. Nichol, P. Jeavons, A. G. Fletcher, R. A. Bonomo, P. K. Maini, J. L. Paul, R. A. Gatenby, A. R. A. Anderson, and J. G. Scott. Steering evolution with sequential therapy to prevent the emergence of bacterial antibiotic resistance. *PLoS Comput Biol*, 11:e1004493, 2015. doi: 10.1371/journal.pcbi.1004493.
- H. A. Orr and R. L. Unckless. Population extinction and the genetics of adaptation. *The American Naturalist*, 172:160–169, 2008.
- H. A. Orr and R. L. Unckless. The population genetics of evolutionary rescue. *PLoS Genet.*, 10(8), August 2014. ISSN 1553-7404. doi: 10.1371/journal.pgen.1004551.

- T. L. Parsons and C. Quince. Fixation in haploid populations exhibiting density dependence ii: The quasi-neutral case. *Theoretical population biology*, 72:468–479, 2007.
- F. Patout, R. Forien, M. Alfaro, J. Papaïx, and L. Roques. The emergence of a birth-dependent mutation rate in asexuals: causes and consequences. *bioRxiv*, 2021.06.11.448026, ver. 3 peer-reviewed and recommended by Peer Community in Mathematical and Computational Biology., June 2021. doi: 10.1101/2021.06.11.448026. URL <https://doi.org/10.1101/2021.06.11.448026>.
- M. Raatz, E. van Velzen, and U. Gaedke. Co-adaptation impacts the robustness of predator–prey dynamics against perturbations. *Ecology and Evolution*, 9(7):3823–3836, 2019. doi: 10.1002/ece3.5006.
- M. Raatz, S. Shah, G. Chitadze, M. Brüggemann, and A. Traulsen. The impact of phenotypic heterogeneity of tumour cells on treatment and relapse dynamics. *PLoS Computational Biology*, 17(2): e1008702, 2021.
- R. Roemhild and H. Schulenburg. Evolutionary ecology meets the antibiotic crisis. *Evolution, Medicine and Public Health*, pages 37–45, 2019.
- R. Roemhild, C. S. Gokhale, P. Dirksen, C. Blake, P. Rosenstiel, A. Traulsen, D. I. Andersson, and H. Schulenburg. Cellular hysteresis as a novel principle to maximize the efficacy of antibiotic therapy. *Proceedings of the National Academy of Sciences*, 2018.
- R. Sender and R. Milo. The distribution of cellular turnover in the human body. *Nature Medicine*, 27(1):45–48, Jan. 2021. doi: 10.1038/s41591-020-01182-9.
- J. D. Sobel. Pathogenesis of urinary tract infection. *Infectious Disease Clinics of North America*, 11(3):531–549, Sept. 1997. doi: 10.1016/S0891-5520(05)70372-X.
- E. Stewart, R. Madden, G. Paul, and F. Taddei. Aging and death in an organism that reproduces by morphologically symmetric division. *PLOS Biology*, 3(2):e45, 2005.
- H. Uecker and J. Hermisson. On the Fixation Process of a Beneficial Mutation in a Variable Environment. *Genetics*, 188(4):915–930, 2011.
- H. Uecker, S. P. Otto, and J. Hermisson. Evolutionary rescue in structured populations. *The American Naturalist*, 183(1):E17 – E35, jan 2014. doi: 10.1086/673914.
- Y. Viossat and R. Noble. A theoretical analysis of tumour containment. *Nature Ecology & Evolution*, Apr. 2021. doi: 10.1038/s41559-021-01428-w.
- P. Virtanen, R. Gommers, T. E. Oliphant, M. Haberland, T. Reddy, D. Cournapeau, E. Burovski, P. Peterson, W. Weckesser, J. Bright, S. J. van der Walt, M. Brett, J. Wilson, K. J. Millman, N. Mayorov, A. R. Nelson, E. Jones, R. Kern, E. Larson, C. J. Carey, Í. Polat, Y. Feng, E. W. Moore, J. VanderPlas, D. Laxalde, J. Perktold, R. Cimrman, I. Henriksen, E. A. Quintero, C. R. Harris, A. M. Archibald, A. H. Ribeiro, F. Pedregosa, P. van Mulbregt, A. Vijaykumar, A. P. Bardelli, A. Rothberg, A. Hilboll, A. Kloeckner, A. Scopatz, A. Lee, A. Rokem, C. N. Woods, C. Fulton, C. Masson, C. Häggström, C. Fitzgerald, D. A. Nicholson, D. R. Hagen, D. V. Pasechnik, E. Olivetti, E. Martin, E. Wieser, F. Silva, F. Lenders, F. Wilhelm, G. Young, G. A. Price, G. L. Ingold, G. E. Allen, G. R. Lee, H. Audren, I. Probst, J. P. Dietrich, J. Silterra, J. T. Webber, J. Slavič, J. Nothman, J. Buchner, J. Kulick, J. L. Schönberger, J. V. de Miranda Cardoso, J. Reimer, J. Harrington, J. L. C. Rodríguez, J. Nunez-Iglesias, J. Kuczynski, K. Tritz, M. Thoma, M. Newville, M. Kümmerer, M. Bolingbroke, M. Tartre, M. Pak, N. J. Smith, N. Nowaczyk, N. Shebanov, O. Pavlyk, P. A. Brodtkorb, P. Lee, R. T. McGibbon, R. Feldbauer, S. Lewis, S. Tygier, S. Sievert, S. Vigna, S. Peterson, S. More, T. Pudlik, T. Oshima, T. J. Pingel, T. P. Robitaille,

- T. Spura, T. R. Jones, T. Cera, T. Leslie, T. Zito, T. Krauss, U. Upadhyay, Y. O. Halchenko, and Y. Vázquez-Baeza. SciPy 1.0: fundamental algorithms for scientific computing in Python. *Nat Methods*, 17(3):261–272, 2020.
- P. Wang, L. Robert, J. Pelletier, W. L. Dang, F. Taddei, A. Wright, and S. Jun. Robust Growth of *Escherichia coli*. *Current Biology*, 20(12):1099–1103, June 2010. doi: 10.1016/j.cub.2010.04.045.
- A. R. Wargo, S. Huijben, J. C. de Roode, J. Shepherd, and A. F. Read. Competitive release and facilitation of drug-resistant parasites after therapeutic chemotherapy in a rodent malaria model. *Proceedings of the National Academy of Sciences*, 104(50):19914–19919, 2007. doi: 10.1073/pnas.0707766104.
- C. J. Watson, A. L. Papula, G. Y. P. Poon, W. H. Wong, A. L. Young, T. E. Druley, D. S. Fisher, and J. R. Blundell. The evolutionary dynamics and fitness landscape of clonal hematopoiesis. *Science*, 367(6485):1449–1454, Mar. 2020. doi: 10.1126/science.aay9333.
- C. Winstanley, S. O’Brien, and M. A. Brockhurst. *Pseudomonas aeruginosa* Evolutionary Adaptation and Diversification in Cystic Fibrosis Chronic Lung Infections. *Trends in Microbiology*, 24(5):327–337, 2016. doi: 10.1016/j.tim.2016.01.008.
- T. K. Wood, S. J. Knabel, and B. W. Kwan. Bacterial Persister Cell Formation and Dormancy. *Applied and Environmental Microbiology*, 79(23):7116–7121, Dec. 2013. doi: 10.1128/AEM.02636-13.
- B. Xue and S. Leibler. Bet Hedging against Demographic Fluctuations. *Physical Review Letters*, 119(10), 2017. doi: 10.1103/PhysRevLett.119.108103.
- A. Yeh and S. Ramaswamy. Mechanisms of cancer cell dormancy-another hallmark of cancer? *Cancer Research*, 75(23):5014–5022, 2015. ISSN 0008-5472. doi: 10.1158/0008-5472.CAN-15-1370.
- B. C. Young, C.-H. Wu, N. C. Gordon, K. Cole, J. R. Price, E. Liu, A. E. Sheppard, S. Perera, J. Charlesworth, T. Golubchik, Z. Iqbal, R. Bowden, R. C. Massey, J. Paul, D. W. Crook, T. E. Peto, A. S. Walker, M. J. Llewelyn, D. H. Wyllie, and D. J. Wilson. Severe infections emerge from commensal bacteria by adaptive evolution. *eLife*, Dec. 2017. doi: 10.7554/eLife.30637.
- H. Yu, L. Lin, Z. Zhang, H. Zhang, and H. Hu. Targeting NF- $\kappa$ B pathway for the therapy of diseases: mechanism and clinical study. *Signal Transduction and Targeted Therapy*, 5(1):1–23, 2020. doi: 10.1038/s41392-020-00312-6.

## A. Supplement

### A.1. Derivation of survival probability fitness component

Recently, [Xue and Leibler \(2017\)](#) derived the extinction risk for a population founded by a small number of individuals. Their model contained also a density-dependent death rate, which makes it slightly different from ours. They set up a master equation and solved it with a generating function approach. For a single initial individual with birth rate  $\beta$  and death rate  $\delta$  they obtain a density-independent extinction risk of

$$q = \frac{\delta}{\beta}$$

from which the survival probability for a new lineage follows as

$$p_{\text{Xue2017}} = 1 - q = 1 - \frac{\delta}{\beta} \quad (\text{S1})$$

Assuming that changes in the population size of the parental lineage are small on the time scale during which the fate of a mutant is decided, i.e. whether it escapes extinction from stochastic drift or not, allows us to fix the total population size to its value when the mutant occurred at time  $T$ . Thus, we can include the density dependence of our model in the survival probability (Eq. S1) by substituting  $\beta \rightarrow \beta \left(1 - \frac{N}{K}\right)$ . This results in a density-dependent survival probability

$$p(T) = 1 - \frac{\delta}{\beta \left(1 - \frac{N(T)}{K}\right)}$$

Including trait-affecting treatment effects and restricting the survival probability to the range between zero and one results in Eq. 6.

A similar derivation uses branching process techniques and arrives at an integral for the fixation probability of a mutant individual on the background of the parental population ([Uecker and Hermisson, 2011](#))

$$p_{\text{fix}}(T) = \frac{2}{1 + \int_T^\infty \left( \beta \left(1 - \frac{N(t)}{K}\right) + \delta \right) \exp \left( - \int_T^t \beta \left(1 - \frac{N(\tau)}{K}\right) - \delta \, d\tau \right) dt}$$

Using the same assumption of  $N(t) = N(T) = \text{const.}$  as above, this reduces to

$$p_{\text{fix}}(T) = 1 - \frac{\delta}{\beta \left(1 - \frac{N(T)}{K}\right)}. \quad (\text{S2})$$

## A.2. Supplementary Figures

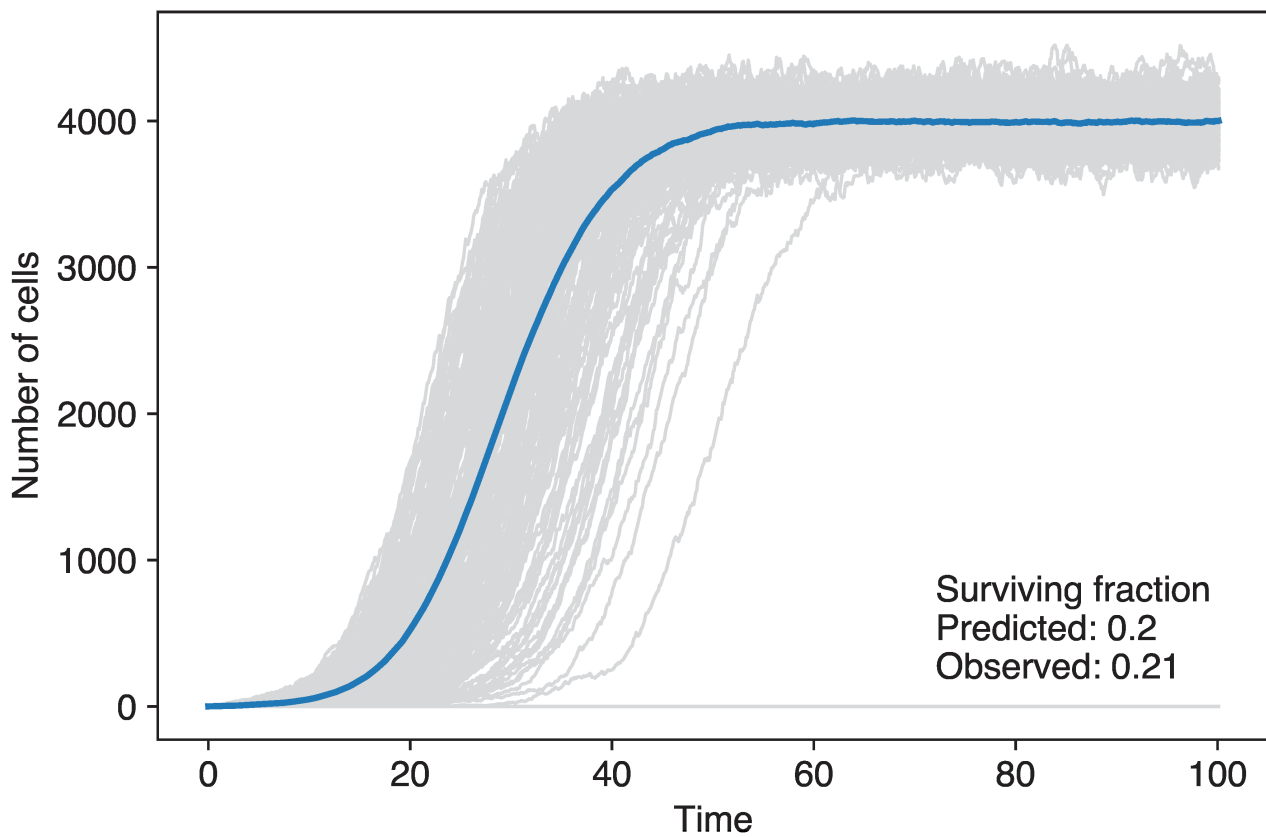


**Figure S1 Numerical simulations of a birth-death process without mutation ( $\mu = 0$ ).** Starting from  $\beta_0 = 1.25$  per time unit and  $\delta_0 = 1.0$  per time unit we find good agreement of the observed survival probability with our survival probability definition. Grey lines are individual replicates, the ~~black dashed~~ blue line is the average over the surviving replicates. We used 1000 replicates,  $dt = 0.1$ ,  $N_0 = 1$  and  $K = 20000$ .

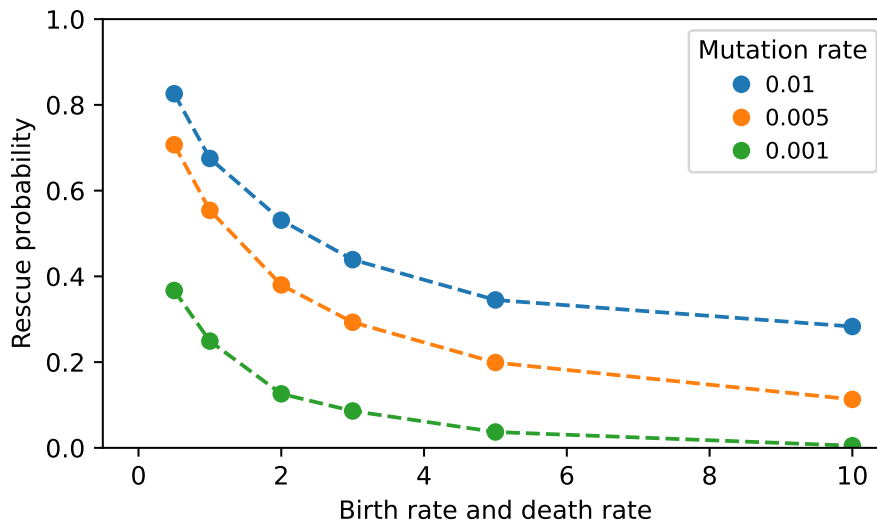


**Figure S2** Effect of ~~initial population size~~ ~~mutation rate~~ on the probability of evolutionary rescue. Smaller ~~initial population size~~ ~~reduces~~ ~~mutation rates~~ ~~reduce~~ the rescue probability. Plot parameters are identical to Fig. 4.

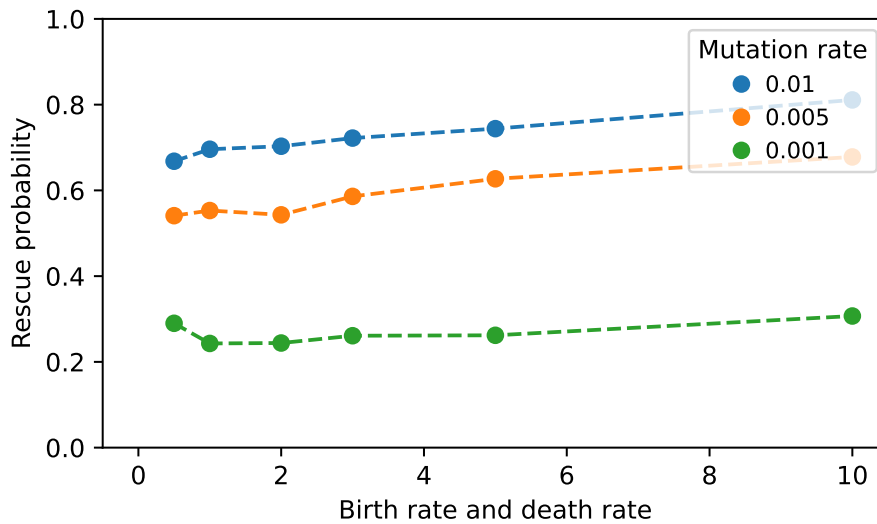


**Figure S3** Probability of evolutionary rescue (multiplicative mutational effect). Parallel to Fig. S2 we tested the effect of multiplicative mutational effects on birth and death rates. The mutant lineages' birth rates here are determined by  $\beta_{\text{mutant}} = \beta_{\text{parental}}(1 + s)$ ,  $s \sim \mathcal{N}(0, \sigma)$ , and death rates are independently determined as  $\delta_{\text{mutant}} = \delta_{\text{parental}}(1 + s)$ ,  $s \sim \mathcal{N}(0, \sigma)$ . Under these assumptions, the rescue probability of initial parental populations is largely independent of turnover.

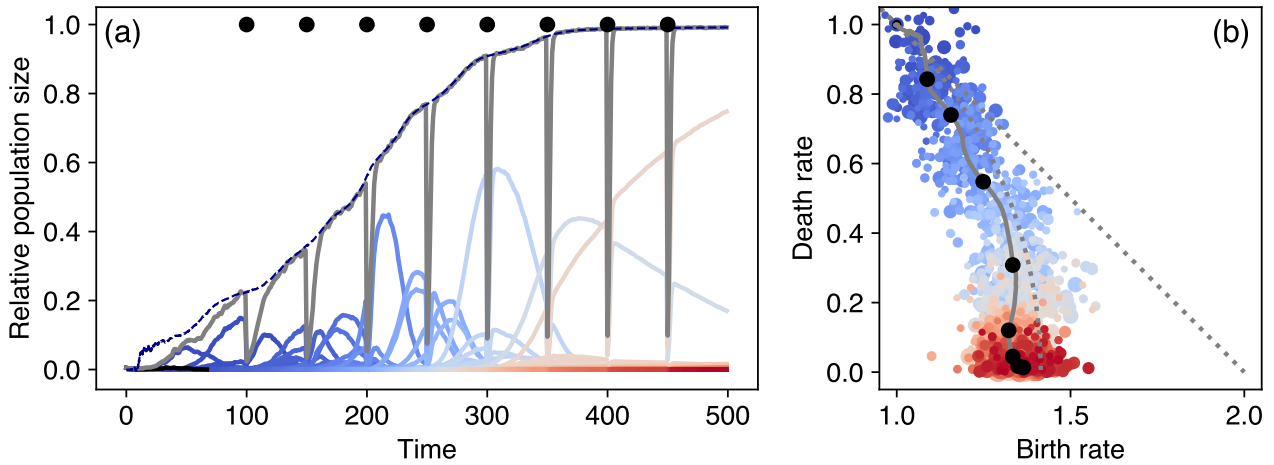


**Figure S4 Exemplary dynamics for bottleneck treatment.** Plot details and parameters as in Fig. 2. Black dots depict the times when the bottleneck instantaneously reduces the population size by a factor  $f = 0.1$ .

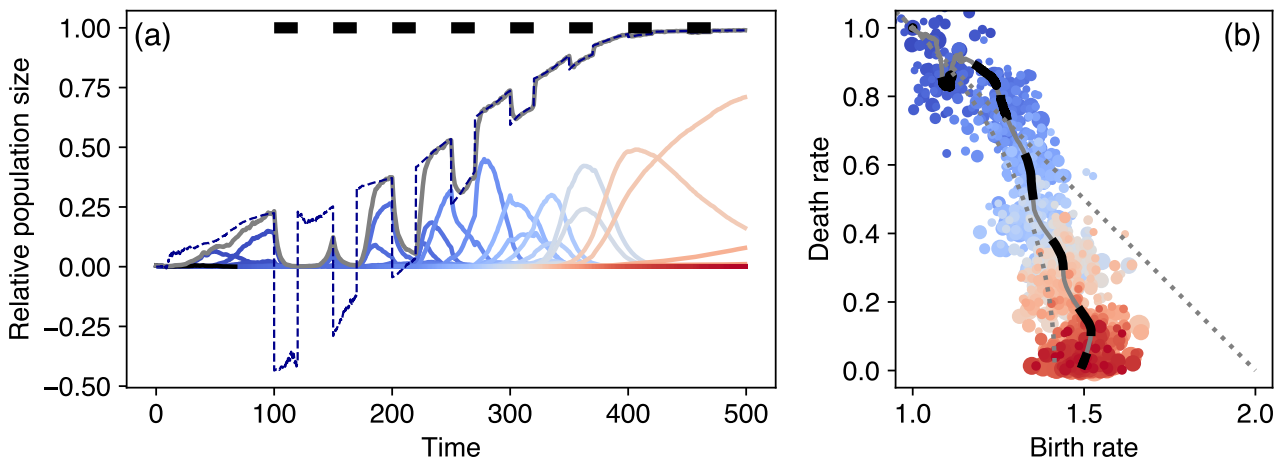


**Figure S5 Exemplary dynamics for static treatment.** Plot details and parameters as in Fig. 2. Black bars depict the times when  $\Delta\beta = 0.5$ . During treatment the effective carrying capacity can reduce to negative values. The population sizes, however, must be non-negative and thus approach zero when the effective carrying capacity becomes negative.



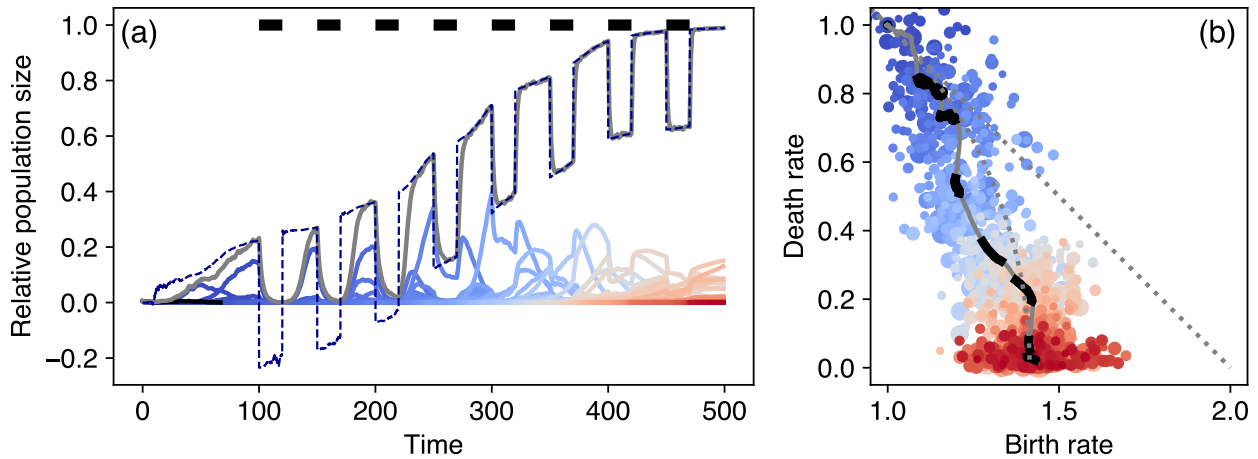


**Figure S6 Exemplary dynamics for toxic treatment.** Plot details and parameters as in Fig. 2. Black bars depict the times when  $\Delta\delta = 0.5$ . During treatment the effective carrying capacity can reduce to negative values. The population sizes, however, must be non-negative values and thus approach zero when the effective carrying capacity becomes negative.

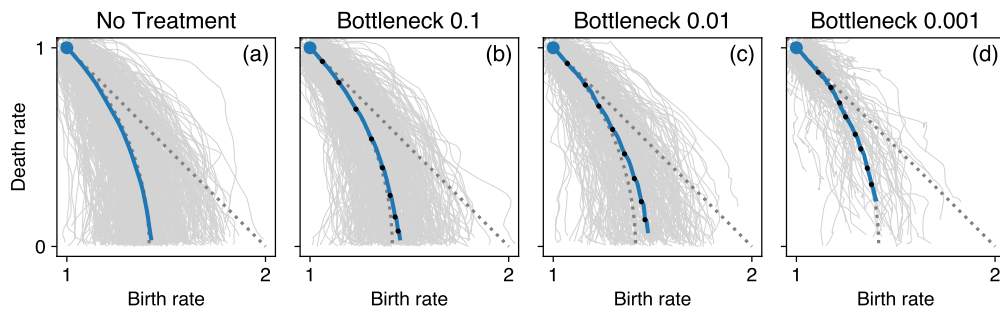


**Figure S7 Trajectories of trait adaptation under density-affecting treatment.** Grey lines represent the 1000 individual replicates. The thick lines show the ensemble average, blue stretches are treatment-off phases, black dots indicate the application of density-affecting treatment.

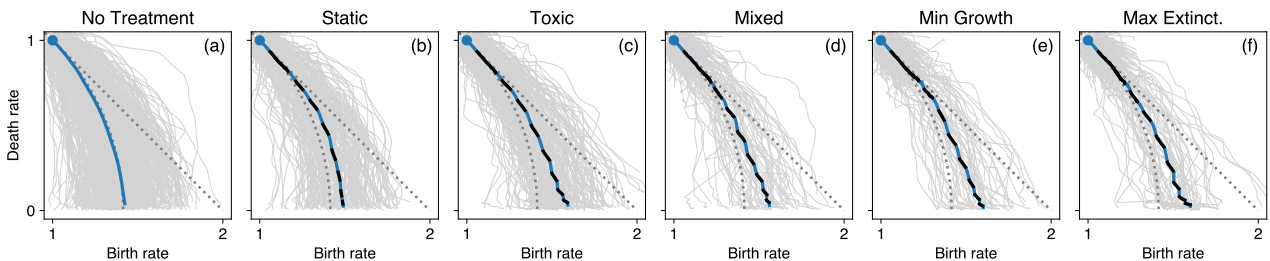


**Figure S8 Trajectories of trait adaptation under trait-affecting treatment.** Grey lines represent the 1000 individual replicates. The thick lines show the ensemble average, blue stretches are treatment-off phases, black stretches indicate treatment-on phases.

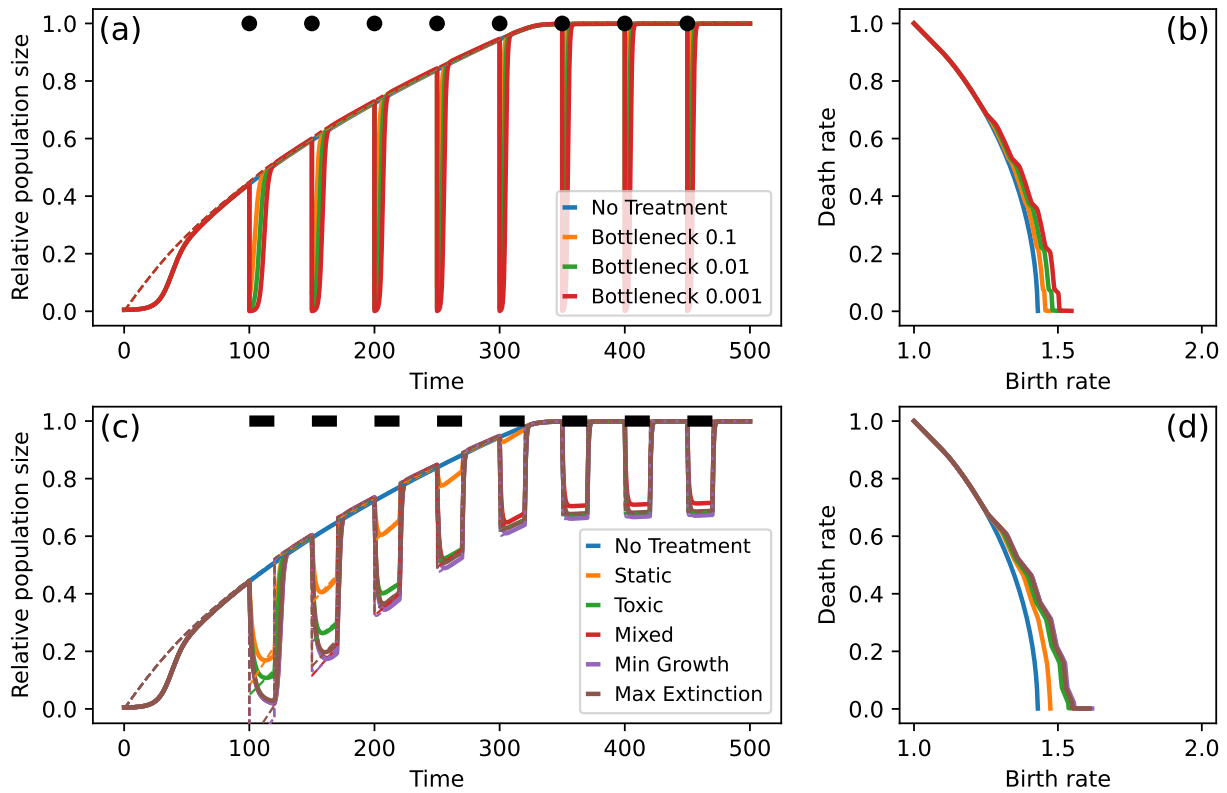


**Figure S9 Deterministic adaptation dynamics under treatment - Net growth fitness gradient.** Choosing the net growth gradient (Eq. (7)) as the fitness gradient in the deterministic model (Eq. (3)) and parameter values from Tab. 1, we obtain adaptation dynamics that are similar to those presented for the stochastic model (Fig. 7).

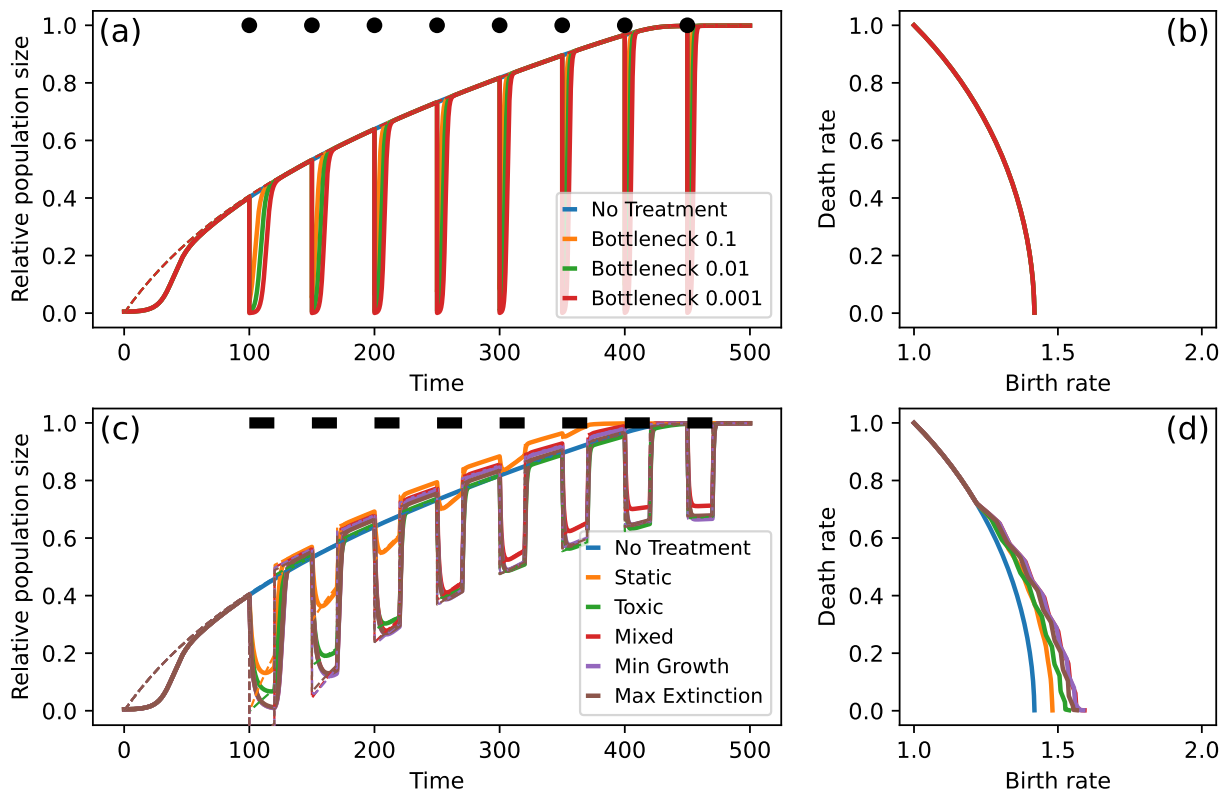


**Figure S10 Deterministic adaptation dynamics under treatment - Survival probability fitness gradient.** Choosing the survival probability gradient (Eq. (8)) as the fitness gradient in the deterministic model (Eq. (3)) and parameter values from Tab. 1, we obtain adaptation dynamics that are similar to those presented for the stochastic model (Fig. 7). However, the density-affecting treatment type has no effect on the trait trajectory as the survival probability fitness gradient is density-independent.

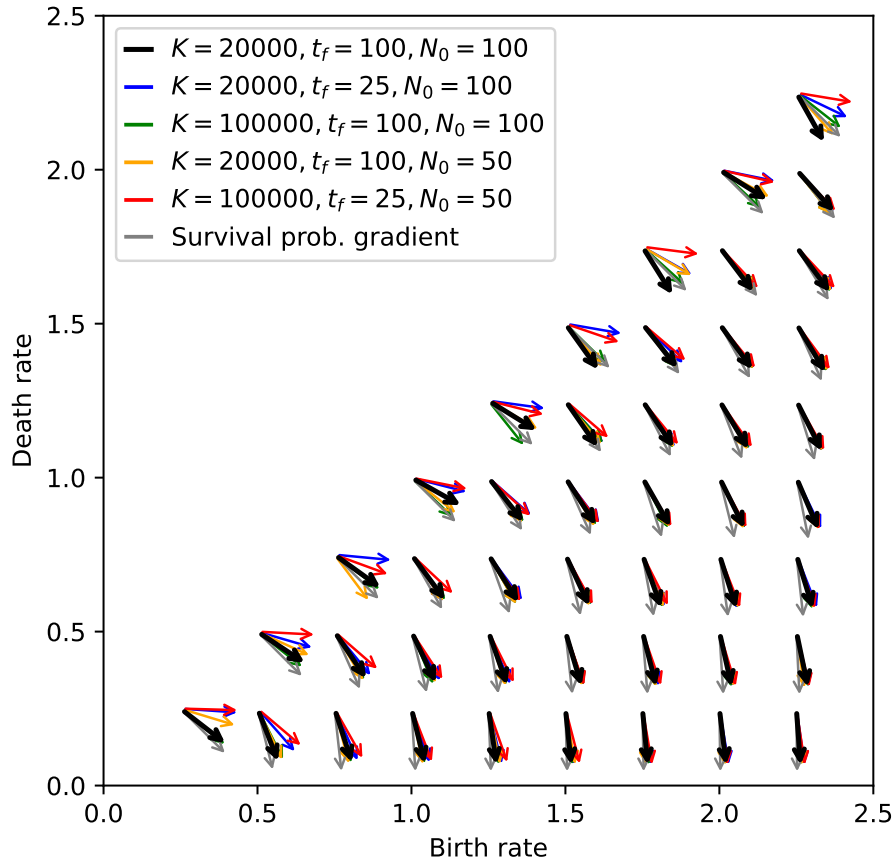


**Figure S11 Observed initial steps of adaptation.** Shown is the average direction of the adaptation trajectories in trait space until time  $t_f$  for different combinations of observation window  $t_f$ , carrying capacity  $K$  and initial population size  $N_0$ . Other parameters are chosen as given by Tab. 1. If the net growth was determining the adaptation trajectory, we expect adaptation steps that have a higher birth-rate component for decreasing density limitation (which can be realized by shorter observational window (blue arrows), higher carrying capacity (green arrows), smaller initial population size (yellow arrows) or all combined (red arrows)). If survival probability (grey arrows) was driving the adaptation we would expect the adaptation direction to not be affected by changes to  $t_f$ ,  $K$  or  $N_0$ .